NASA Technical Memorandum 72865

CORRELATION OF PREDICTED AND MEASURED THERMAL STRESSES ON AN ADVANCED AIRCRAFT STRUCTURE WITH DISSIMILAR MATERIALS

Jerald M. Jenkins

June 1979

NASA

NASA Technical Memorandum 72865

CORRELATION OF PREDICTED AND MEASURED THERMAL STRESSES ON AN ADVANCED AIRCRAFT STRUCTURE WITH DISSIMILAR MATERIALS

Jerald M. Jenkins

Dryden Flight Research Center
Edwards, California

National Aeronautics and
Space Administration

1979

CORRELATION OF PREDICTED AND MEASURED THERMAL STRESSES ON AN ADVANCED AIRCRAFT STRUCTURE WITH DISSIMILAR MATERIALS

Jerald M. Jenkins
Dryden Flight Research Center

INTRODUCTION

Several operational aircraft have accumulated significant flight time at speeds sufficient to produce severe aerodynamic heating (refs. 1 to 3). Even with this experience, there exists a lack of understanding of how accurately thermal stresses can be predicted on a complex structure. The ability to predict thermal stresses accurately has great impact on both the safe magnitude of stresses and the long-term effect of thermal cycling on the structure. An effort to study how well thermal stresses could be predicted in detail was begun in reference 4 and continued in reference 5. This paper provides the third and last part of this particular study about how laboratory measured thermal stresses compare with thermal stresses predicted using NASA structural analysis (NASTRAN) computer models.

A test structure representing a portion of a hypersonic vehicle (ref. 6) was instrumented with strain gages and thermocouples. This test structure was then subjected to laboratory heating representative of hypersonic flight conditions. Two finite element computer models of this structure were developed using bar and shear panel elements of the NASTRAN program (ref. 7). Temperature inputs from the tests were used to predict model thermal stresses, and these were correlated with the test measurements.

DESCRIPTION OF TEST SPECIMEN AND INSTRUMENTATION

A test specimen resulted from work directed toward studying the feasibility of a hypersonic research airplane (ref. 6). One structural concept resulting from this study was a heat sink type of structure. The basic philosophy was to use a variable-thickness, load-carrying skin to absorb heat as required to maintain a certain skin temperature. The skin was supported by a titanium zee substructure as shown in figure 1. A beryllium-aluminum composite metal (ref. 8) was selected as the skin because of the light weight and large thermal capacity of beryllium. The substructure frames were a zee-type configuration with titanium being used as the zee material. A photograph of the substructure frames is shown in figure 2. A photograph of the complete specimen is shown in figure 3 where the skins are attached to the substructure.

The location of the temperature and strain instrumentation is shown in figure 4. Seventeen thermocouples and seventeen strain gages were used for analysis purposes in this paper. Five thermocouples and strain gages were located on the skins, while the remaining twelve were located at strategic points on the substructure. Thermocouples and foil-type strain gages were used in the test temperature environment, which ranged from 232° K (-42° F) to 633° K (679° F).

TEST PROCEDURE

The general test setup is shown in the schematic in figure 5. The specimen is completely encased but is supported so that it is unrestrained--in other words, the edges are free to rotate and translate in the plane of the skin. A rack of radiant heaters (ref. 9) is located such that the skins can be heated on the side away from the frames. A blower system is situated such that a mixture of air and gaseous nitrogen can be blown over the specimen if cooling is desired.

A flight profile for a hypersonic mission is shown in figure 6. The profile is of a 6-minute rocket-powered mission (ref. 6) with a 1-minute cruise at Mach 6. Skin temperatures were calculated based on the computer program identified in reference 10.

A time history of skin temperature of the profile was used to perform the test. The test specimen is cooled prior to heating to simulate the cold soak condition that occurs when rocket powered aircraft are air launched at high altitude.

After the specimen is cooled, the heating is started by controlling the skin temperatures with radiant heaters according to the prescribed temperature time history.

DESCRIPTION OF THE STRUCTURAL MODELS

An initial NASTRAN model (shown in figure 7) was developed for one of the symmetrical quarters of the structure. This model, designated ASTEEL, was a 97 element model constructed of NASTRAN bar and shear panel elements. The 97 element ASTEEL model was composed of 73 bar elements and 24 shear panel elements. In constructing the model, 50 grid points were used with 231 degrees of freedom, 69 single point constraints, and 250 bulk data cards. Since the ASTEEL model was constructed of very long elements, an additional model, designated CSTEEL, was developed with a significantly changed grid arrangement. The CSTEEL model (shown in figure 8) contained 129 bar elements and 54 shear panel elements. In constructing the model, 76 grid points were used with 387 degrees of freedom, 69 single point constraints, and 402 bulk data cards. The NASTRAN models, which represented one symmetrical quarter of the test specimen, each have a surface area of 0.34 square meter (3.68 square feet) and a nominal depth of 0.10 meter (4 inches). The grid numbering system common to both the ASTEEL and CSTEEL models is shown in figure 9.

RESULTS

The results of the hypersonic heating simulation will be examined from the viewpoint of the thermal stress distribution at a single instant of time and from the viewpoint of the time-history of thermal stress at discrete points.

Time histories of temperatures and thermal stress measured during the laboratory heating test for each of the locations shown in figure 4 are presented in figure 10 as the solid lines. The time histories of temperature generally begin at a low value representing a high altitude soak condition. The temperatures then rise to some higher value reflecting a maximum Mach 6 heating environment. The time histories of thermal stresses are compared with the ASTEEL and CSTEEL NASTRAN models. The variation in the calculated thermal stresses results from longitudinal temperature variations (Y-direction). Since the ASTEEL model has only one element in the Y-direction, there is no way of accounting for temperature variations in that direction. The CSTEEL model has three elements in the Y-direction, hence, temperature variations in the Y-direction could be considered.

Thermal stresses in the skin are presented in figures 10(a) through 10(e). Frame thermal stresses are presented in figures 10(f) through 10(q). It can be seen that the correlation of the measured test data with the NASTRAN models is highly varied. There is significant difference between the measured and calculated thermal stresses at locations such as is shown in figures 10(f) and 10(l). There is very close agreement between the measured and calculated thermal stresses in other cases such as shown in figures 10(h), 10(m), and 10(n).

The distribution of measured thermal stress is shown in figure 11 for four different instants of time. The distribution in the left frame and the right frame is shown in the upper plots. The distribution in the skin is shown in the lower plot. The measured thermal stress data is compared to both the calculations from the ASTEEL and CSTEEL models.

Temperature Smearing

A general problem is becoming apparent in the analysis of large structures for thermal stress. The amount of temperature information seems likely to lag the structural input requirement. The test structure in this paper is a prime example of this problem. The ASTEEL model has 50 grid points and the CSTEEL model has 76 grid points. Each of these grid points requires a temperature input. There were available only 17 thermocouples at the strain gage locations plus two other control thermocouples (see figure 12). The available test data supplied only a small percentage of the temperature information potentially required as direct input to the grid points of the structural model. Somehow, the 19 temperatures may have to be expanded to 50 in the case of the ASTEEL model and to 76 for the CSTEEL model. The technique for deducing the temperatures at the grid points for which no direct temperatures are available is known as temperature smearing.

Temperature smearing is necessary when the temperature distribution of the structure is non-uniform, unsymmetrical, or otherwise incomplete. The temperatures for the test structure in this paper were significantly non-uniform as can be seen in figure 13. The numbers in the panel squares represent the temperature at the center of each of the panels at the four minute time slice (see figure 6). It can be seen that no symmetry exists in the temperature distribution of the specimen. Hence, a problem exists when the model represents only one quarter of a structure that does not have an identical (or mirror image) temperature pattern in the other three quarters.

The typical manner in which temperatures were smeared is shown in figures 14 and 15. In figure 14(a), the temperature along the longitudinal line connecting grid points 25, 125, and 225 and 27 are shown. Along this line there were only two temperature

measurements recorded during the laboratory test; at grid points 25 and 225. These measured temperatures are represented by the two circular symbols. The temperatures for the ASTEEL model were considered to not vary in the longitudinal direction (from grid point 25 to grid point 27), hence, the temperature distribution for the ASTEEL model is represented by the straight, dashed line. The solid line passing through the two measured points represents the temperature smearing used for the CSTEEL model. A similar plot is shown in figure 14(b) for a line connnecting grid points 1, 101, 201, and 3. Along this line there were only two temperature measurements; at grid points 1 and 201. The dashed line represents the temperature used for the ASTEEL model. The solid line represents the smeared temperature distribution used for the CSTEEL model.

The lateral temperature smearing is shown in figure 15. It can be seen that several measured temperatures are available along the line connecting grid points 37 and 1. The distribution of temperature input to the ASTEEL and CSTEEL models is identical along this line. There is much less temperature data along the line connecting grid points 237 and 201. The CSTEEL model is smeared through the two available temperature data points. The ASTEEL temperature distribution (dashed line) is seen to vary significantly from the distribution used for the CSTEEL model. This is because the ASTEEL temperatures along grid points 237 to 201 are a direct extension of the temperatures along grid points 37 to 1.

More sophisticated smearing techniques can be established. The basic measured temperature data can be smeared to other grid points using supporting calculative techniques. However, for this test specimen, there was little justification for more effort than the linear interpolations and curve fitting techniques that were used.

DISCUSSION

The primary purpose of this paper has been to evaluate how well thermal stress could be predicted on a heated laboratory test structure constructed of dissimilar materials. Predictions were generated using the finite element NASTRAN models ASTEEL and CSTEEL. The manner in which temperatures were smeared was found to have great impact on the correlation of test data with predictions.

The basic correlation data is presented in figures 11(a) through 11(d) in a generally condensed form. The stresses in the two spars were predicted quite well except near the interface with the skins. The measured stresses near the skin juncture

on the right frame are near 210 MN/m^2 (30 Klb/in^2) while the NASTRAN calculated stresses are less than 35 MN/m^2 (5 Klb/in^2). A similar situation exists for the left frame, however, the discrepancy is not as large in magnitude. The two structural models (ASTEEL and CSTEEL) produced very similar answers in the frames for all time segments.

Thermal stresses in the skin compare closely with the NASTRAN models for the zero and two minute time segments. At time = 4 minutes the thermal stresses calculated with the two finite element models do not agree with each other and they do not agree with the measured thermal stresses. It can be seen that variations as high as 62 MN/m^2 (9 Klb/in^2) between the ASTEEL and CSTEEL models exist. This reflects the problem associated with smearing the temperature adequately. It can also be seen that the thermal stress data calculated using the NASTRAN models does not agree closely with the measured thermal stresses at time = 4 minutes. The calculated thermal stresses at time = 6 minutes also disagree somewhat with the measured data, however, there is closer agreement between the two models.

It is apparent from the results presented in this paper and the results of reference 5 that the thermal stresses calculated using the NASTRAN models are very sensitive to minor variations in the temperatures input to the node points. It was shown that smearing temperatures in more detail, as was done for the CSTEEL model, does provide a different answer from the more coarse temperature smearing of the ASTEEL model. Insufficient information is available to determine the extent to which additional temperature information would aid in comparing with the measured values. The general comparison of calculated and measured thermal stresses is quite good and there is little doubt that the finite element approach provided by NASTRAN results in correct thermal stress calculations. There were some local discrepancies that could be attributed to either inadequate temperature information or insufficient NASTRAN elements in the local area.

The areas in which the NASTRAN models failed to predict the thermal stresses accurately were in the frame-skin juncture areas and in the skins themselves. These inadequacies could have great impact on the long term life of an airplane. The large measured thermal stresses at the frame-skin juncture are most pronounced at time = 0 minutes. These stresses most likely result from the contraction of dissimilar materials (i.e. the titanium frames and the beryllium/aluminum skins) at this low temperature soak condition. The general inability to predict thermal stresses at this point is apparent all through the time-history of the hypersonic test (see figures 10(f), 10(l), and 11). Large and unpredicted thermal stresses in this particular area could have great impact on the ultimate life of fasteners used at this juncture. Local buckling, yielding, and fatigue problems could cause serious problems in

the fastener area. It is felt that the discrepancies occurring at the skin/frame juncture were most likely due to insufficient modeling elements rather than temperature problems.

The discrepancy between measured and calculated thermal stresses in the skin area was not a large discrepancy in terms of magnitude. However, minor unknowns in terms of skin stresses for hot structures can have serious consequences. Skins are very susceptible to buckling because of prevailing compressive thermal stresses and stiffness degradation due to high temperature. The high temperature of the skins also creates the environment for creep problems if the stresses are not accurately known. The calculated thermal stresses in the skin areas exhibited distinct sensitivity to temperature smearing variations. It is felt that the problems with predicting skin thermal stresses with the NASTRAN models was more likely attributed to inadequate temperature inputs rather than modeling insufficiencies.

The ASTEEL model was developed with 97 bar and shear panel elements. The model contained approximately 285 elements per square meter (27 elements per square foot) of surface area. Approximately 147 temperature inputs per square meter (14 per square foor) of surface area were used to develop predicted thermal stresses. The CSTEEL model had 183 bar and shear panel elements. There were approximately 540 elements per square meter (50 elements per square foot) of surface area. The element density was considered adequate to predict the distribution of thermal stress and the time histories of thermal stress reliably. Approximately 224 temperature inputs per square meter (21 per square foot) of surface area were required to develop predicted thermal stresses.

CONCLUDING REMARKS

Several important problems were addressed in this paper. A structure fabricated of dissimilar materials was investigated in terms of correlating measured and calculated thermal stresses. Additional information was added to a growing data base from which estimates of finite element model complexities can be made with respect to thermal stress analysis. The manner in which temperatures were smeared to the finite element grid points was examined from the point of view of the impact on thermal stress calculations.

The general comparison of calculated and measured thermal stresses is quite good and there is little doubt that the finite element approach provided by NASTRAN results in correct thermal stress calculations. Discrepancies did exist between measured and calculated values in the skin and the skin/frame junctures. The problems with predicting skin thermal stresses were attributed

to inadequate temperature inputs to the structural model rather than modeling insufficiencies. The discrepancies occurring at the skin/frame juncture were most likely due to insufficient modeling elements rather than temperature problems.

In some areas, calculated thermal stresses varied considerably due to different temperature smearing approaches. It is apparent from the results of this paper, that thermal stresses calculated using the NASTRAN models are very sensitive to minor variations in the temperature input to the grid points.

The more sophisticated NASTRAN model (CSTEEL) was developed with 183 bar and shear panel elements. The model contained approximately 540 elements per square meter (50 elements per square foot) of surface area. The element density was considered adequate to predict the distribution of thermal stress and the time histories of thermal stress reliably. Approximately 224 temperature inputs per square meter (21 per square foot) of surface area were required to develop predicted thermal stresses.

Dryden Flight Research Center
National Aeronautics and Space Administration
Edwards, Calif., June 6, 1979

REFERENCES

1. Quinn, Robert D.; and Olinger, Frank V. (appendix A by James C. Dunavant and Robert L. Stallings, Jr.): Heat-Transfer Measurements Obtained on the X-15 Airplane Including Correlations With Wind Tunnel Results. NASA TM X-1705, 1969.

2. Andrews, William H.: Summary of Preliminary Data Derived From the XB-70 Airplanes. NASA TM X-1240, 1966.

3. Quinn, Robert D.; and Olinger, Frank V.: Flight Temperatures and Thermal Simulation Requirements. NASA YF-12 Flight Loads Program. NASA TM X-3061, 1974, pp. 145-183.

4. Jenkins, Jerald M.; Schuster, Lawrence S.; and Carter, Alan L.: Correlation of Predicted and Measured Thermal Stresses on a Truss-Type Aircraft Structure. NASA TM-72857, November, 1978.

5. Jenkins, Jerald M.: Correlation of Predicted and Measured Thermal Stresses On An Advanced Aircraft Structure With Similar Materials. NASA TM-72862, April, 1979.

6. Combs, H. G., et al.: Configuration Development Study of the X-24C Hypersonic Research Airplane - Executive Summary. NASA

CR 145274, 1977.

7. McCormick, Caleb W.,ed.: The NASTRAN User's Manual (Level 15). NASA SP-222(01), 1972.

8. Aerospace Structural Metals Handbook. Volume 4 - Non-Ferrous Alloys. ADML-TR-68-115, Air Force Materials Lab., Wright-Patterson AFB, 1978.

9. Sefic, Walter J.; and Anderson, Karl F.: NASA High Temperature Loads Calibration Laboratory. NASA TM X-1868, 1969.

10. Gord, P. R.: Measured and Calculated Structural Temperature Data From Two X-15 Airplane Flights With Extreme Aerodynamic Heating Conditions. NASA TM X-1358, 1967.

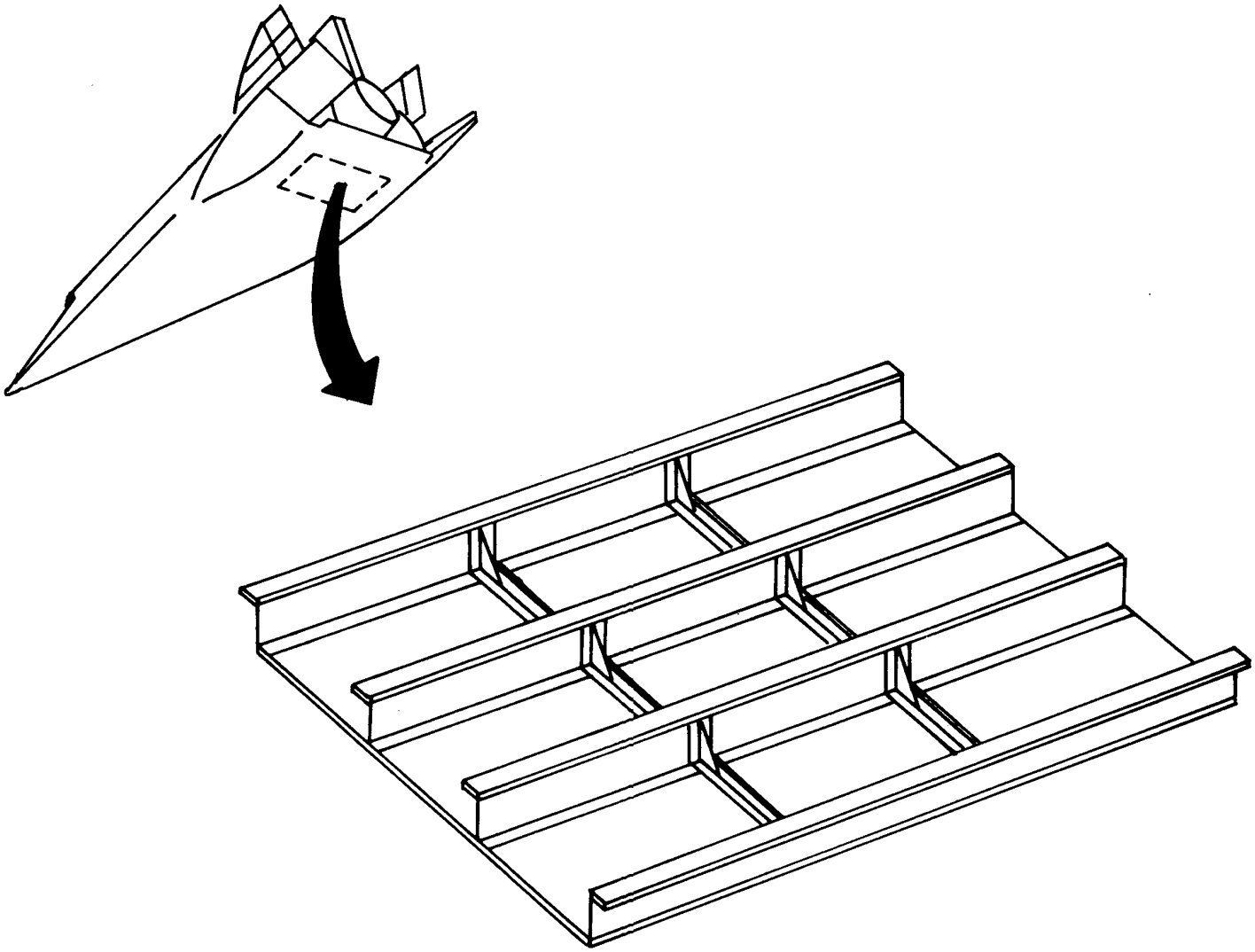

Figure 1. Location of test specimen on hypothetical hypersonic airplane.

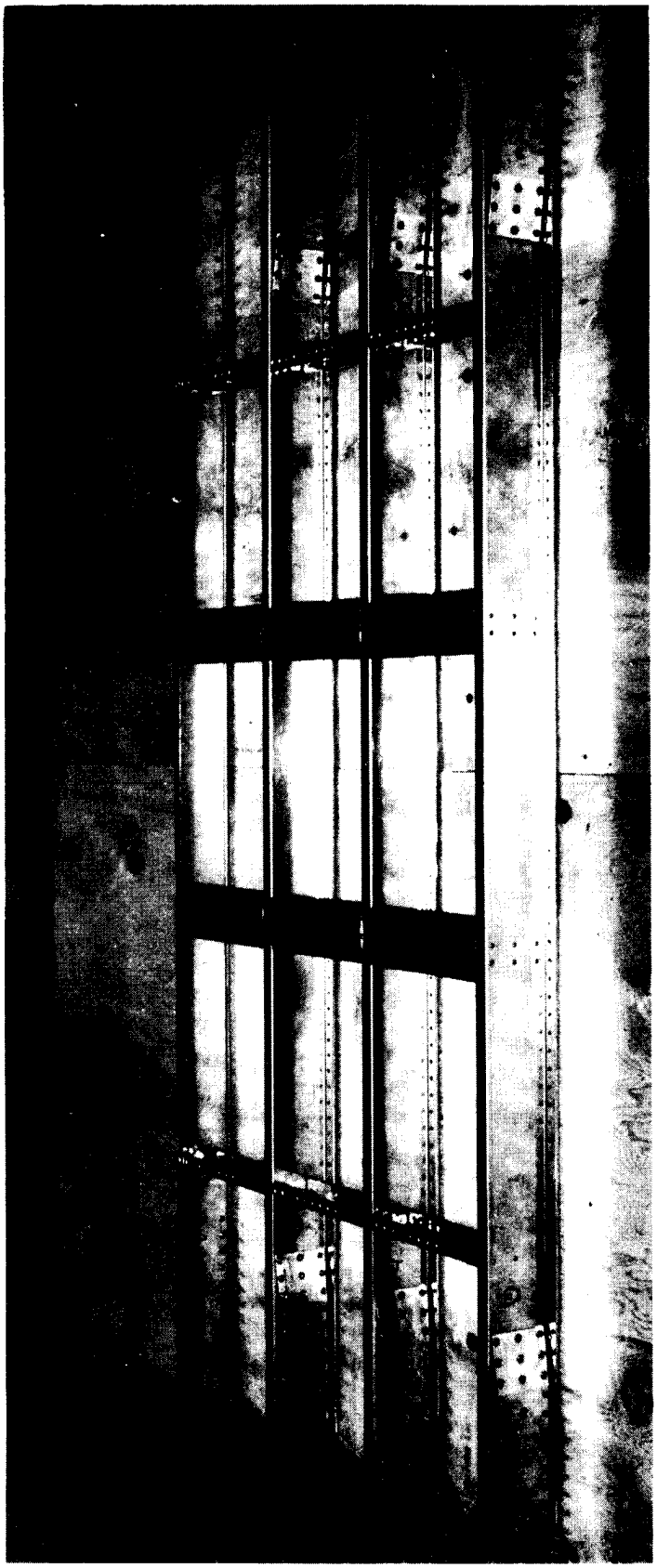

E-31363

Figure 2. Titanium zee substructure frames.

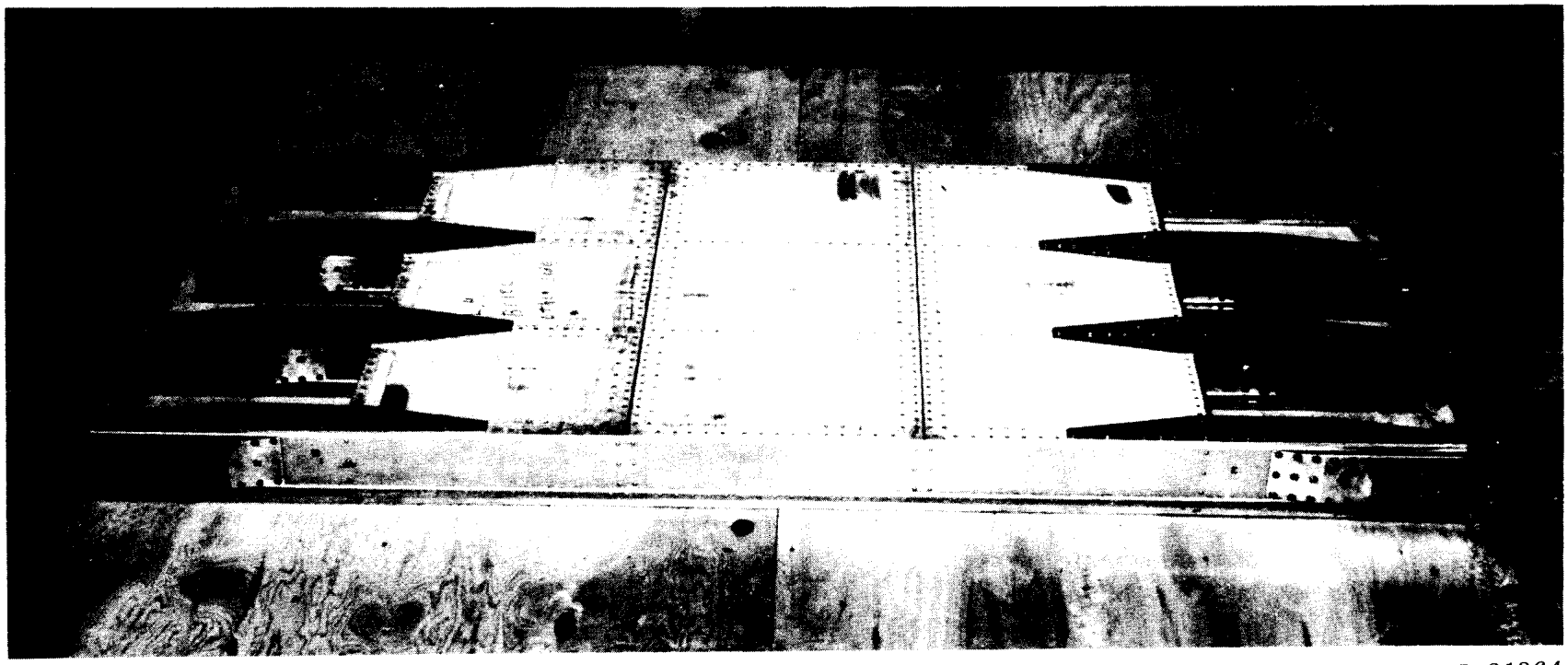

E-31364

Figure 3. Titanium zee/beryllium-aluminum skin test component.

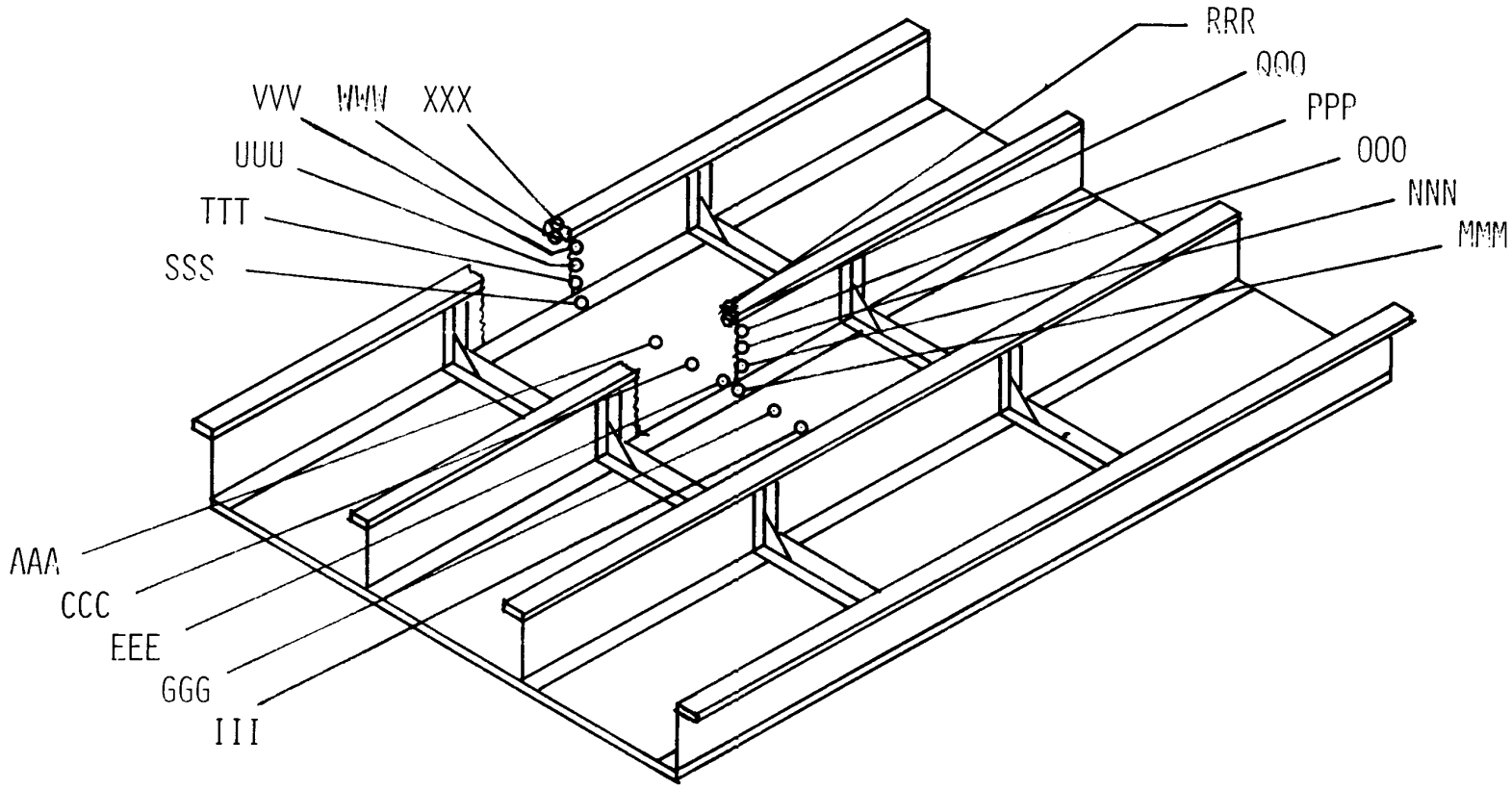

Figure 4. Location of strain gages and thermocouples used for analysis.

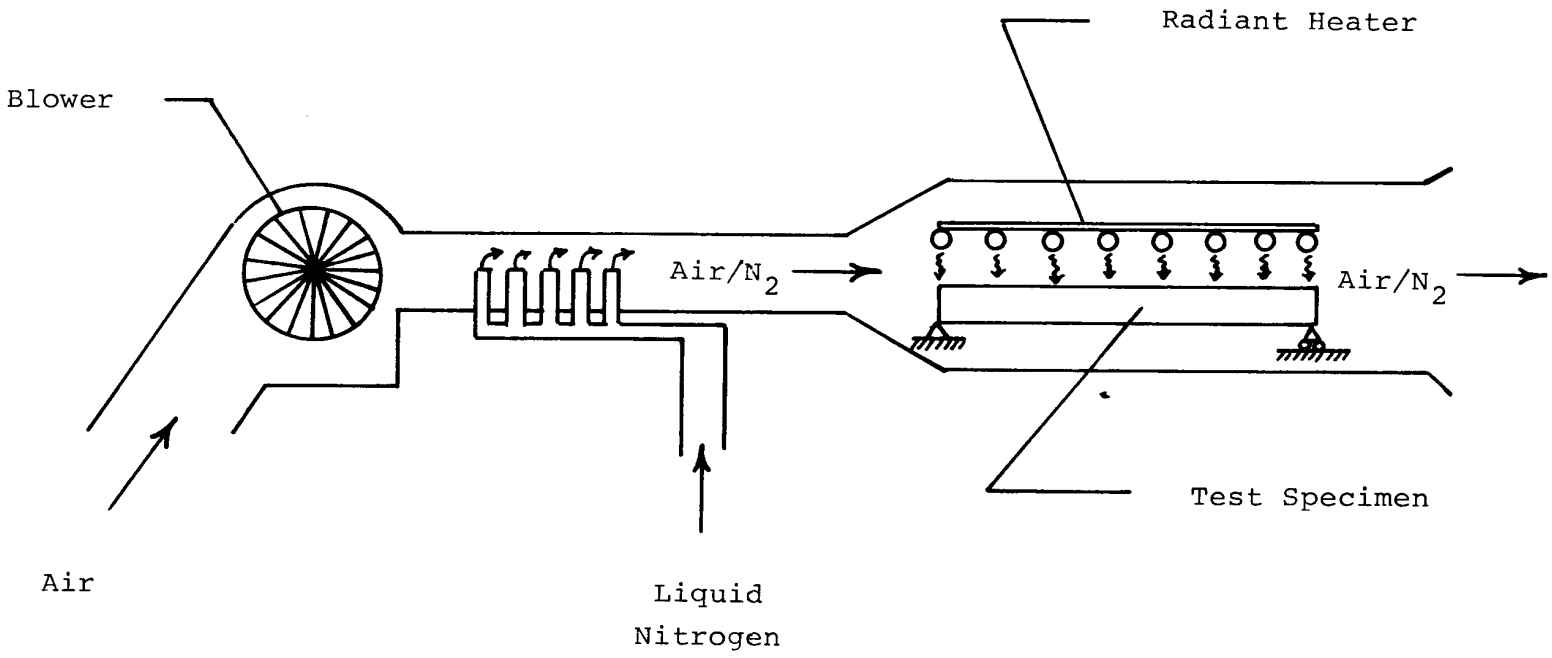

Figure 5. Schematic illustrating the general test setup.

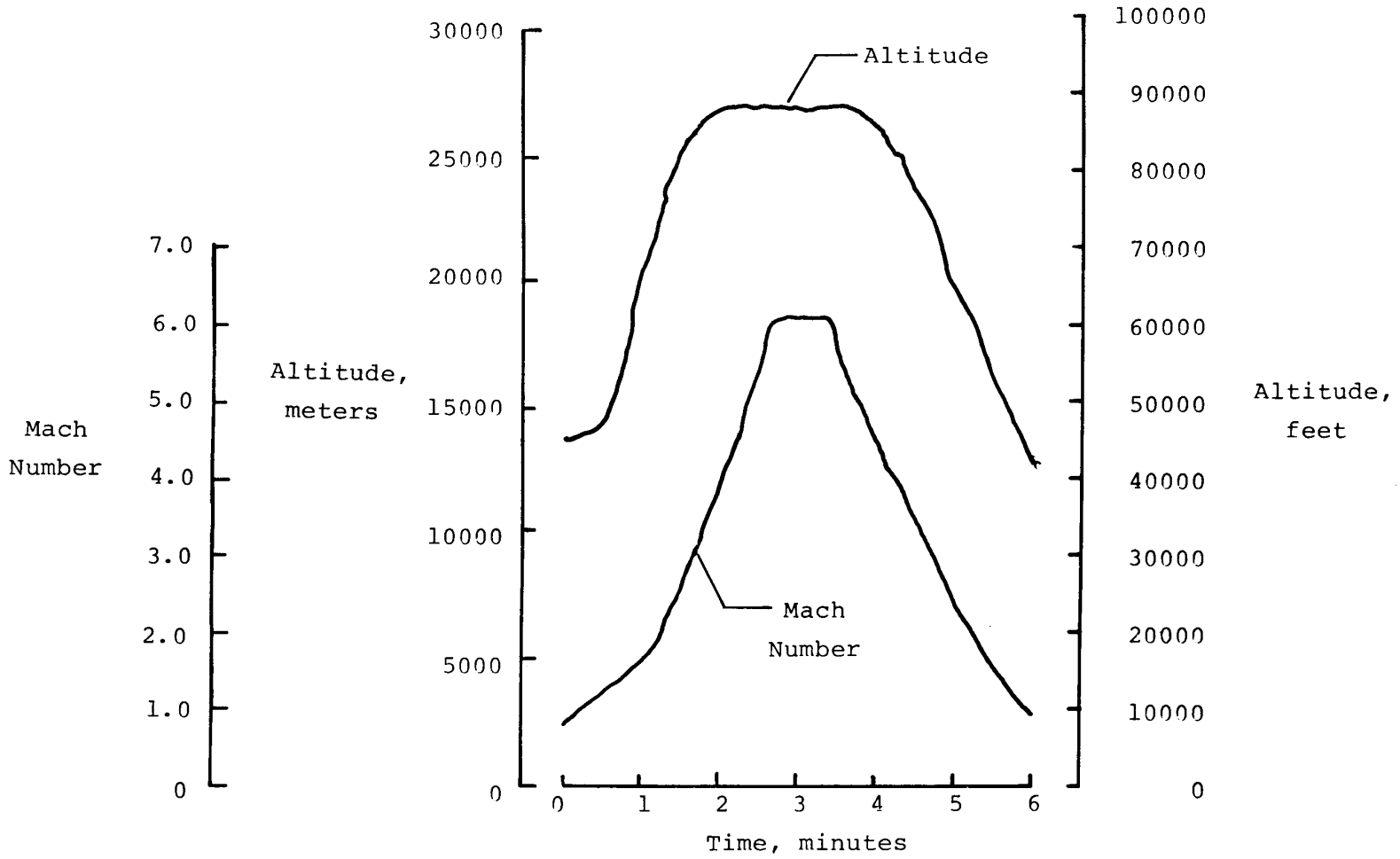

Figure 6. Time history of altitude and Mach number for a hypersonic flight.

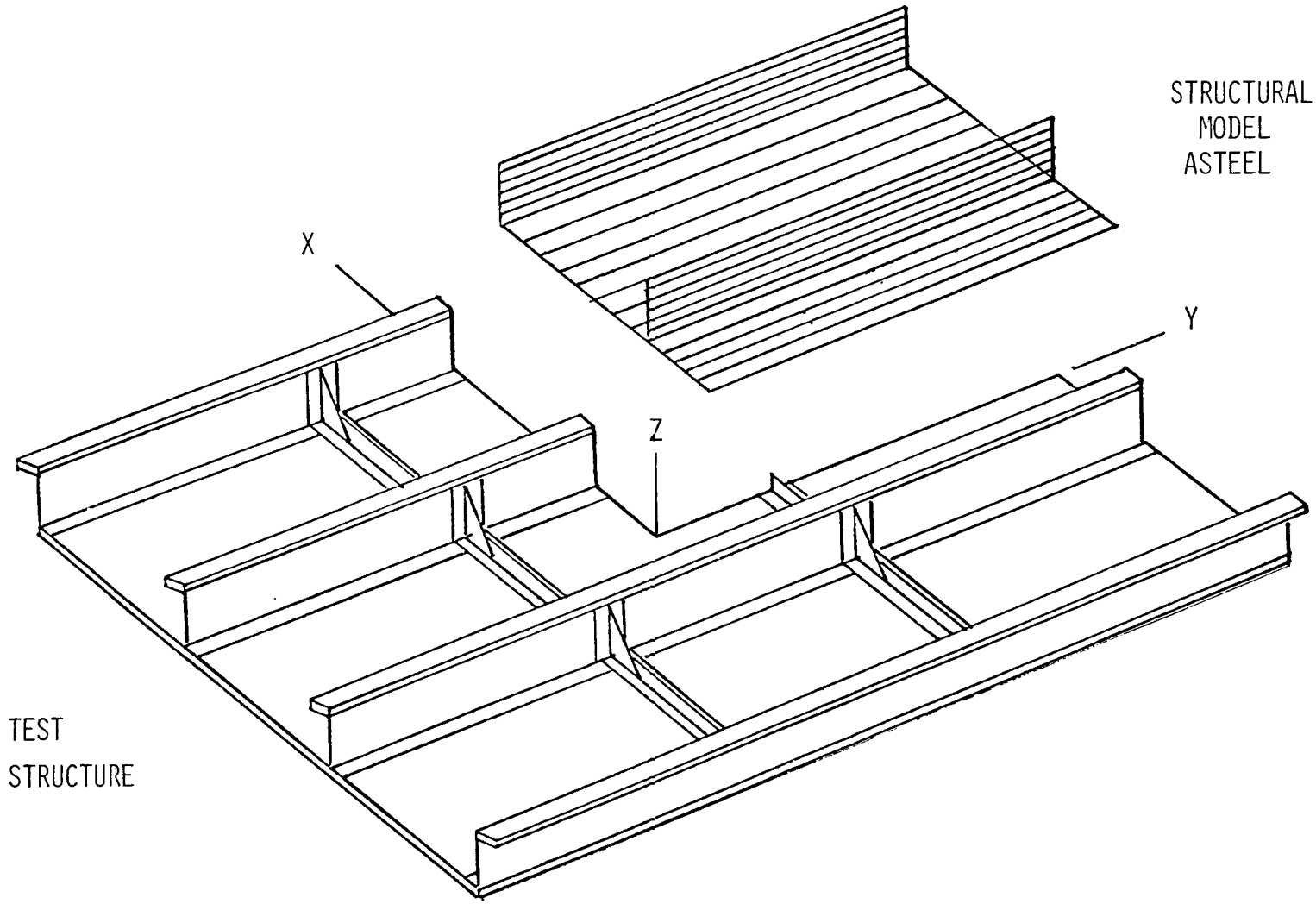

Figure 7. Test structure showing location of structural model.

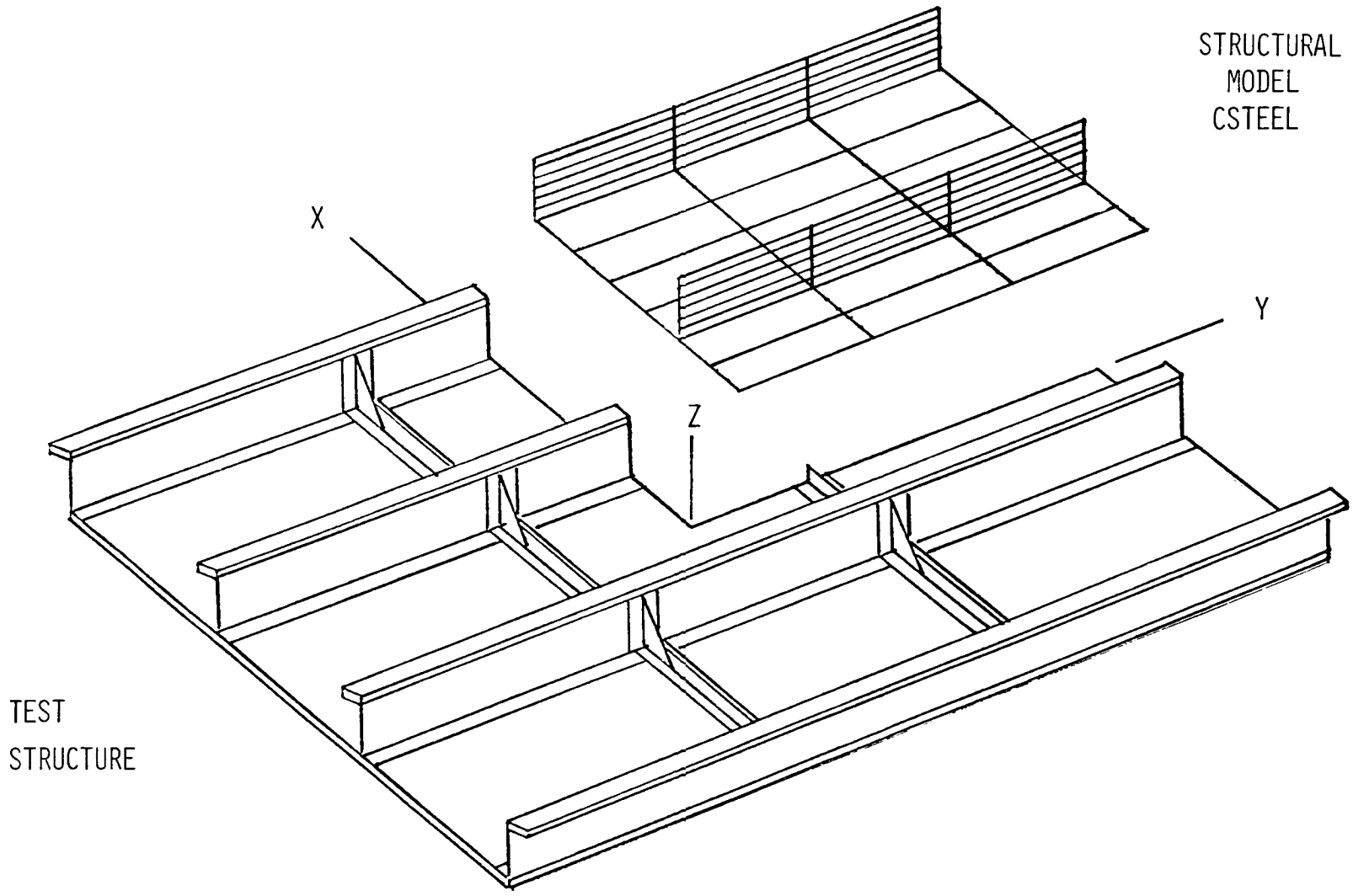

Figure 8. Test structure showing location of structural model.

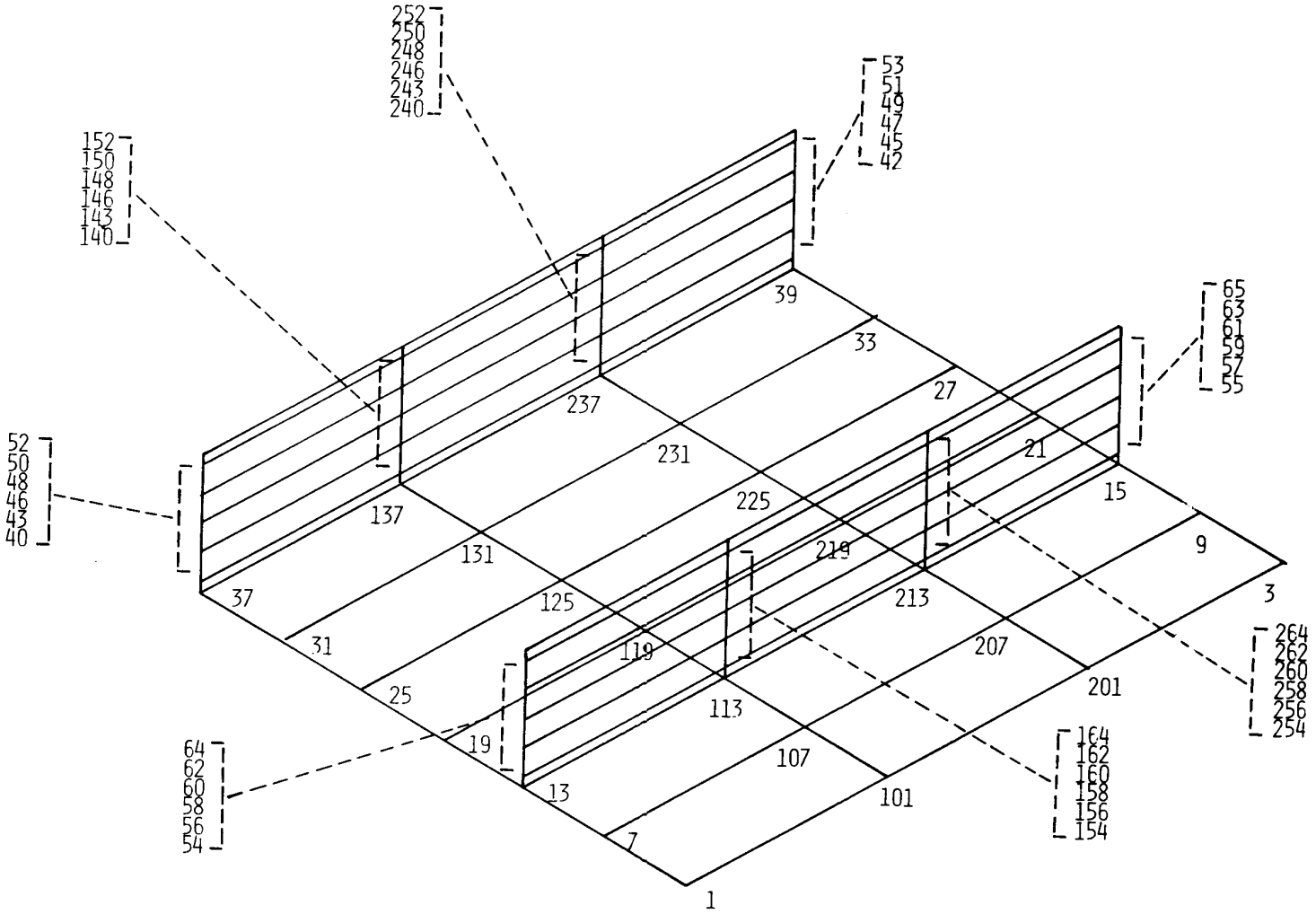

Figure 9. Grid point numbering system for NASTRAN models.

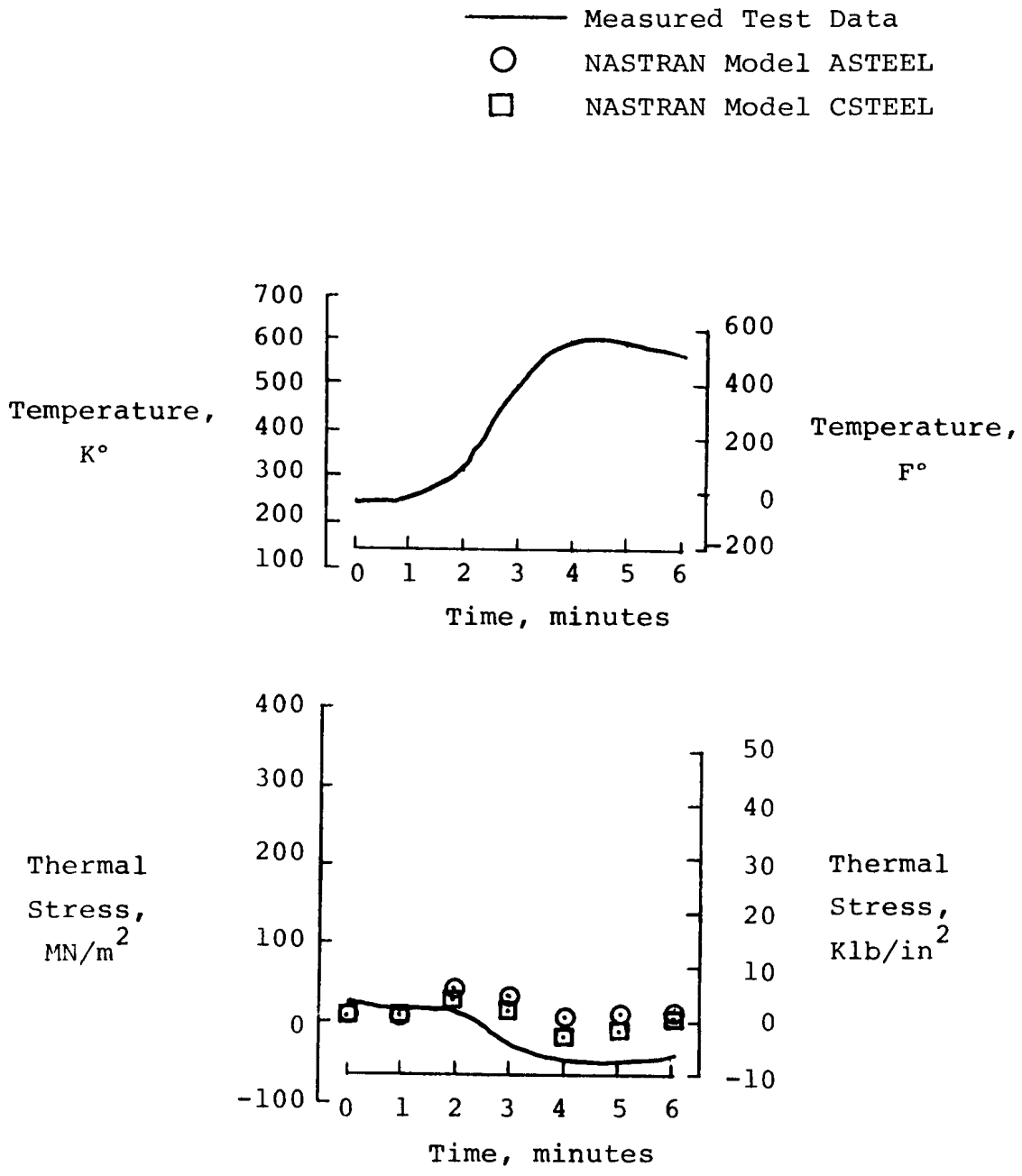

(a) Location AAA.

Figure 10. Measured temperatures and comparison of measured and NASTRAN-calculated thermal stresses for hypersonic heating simulation.

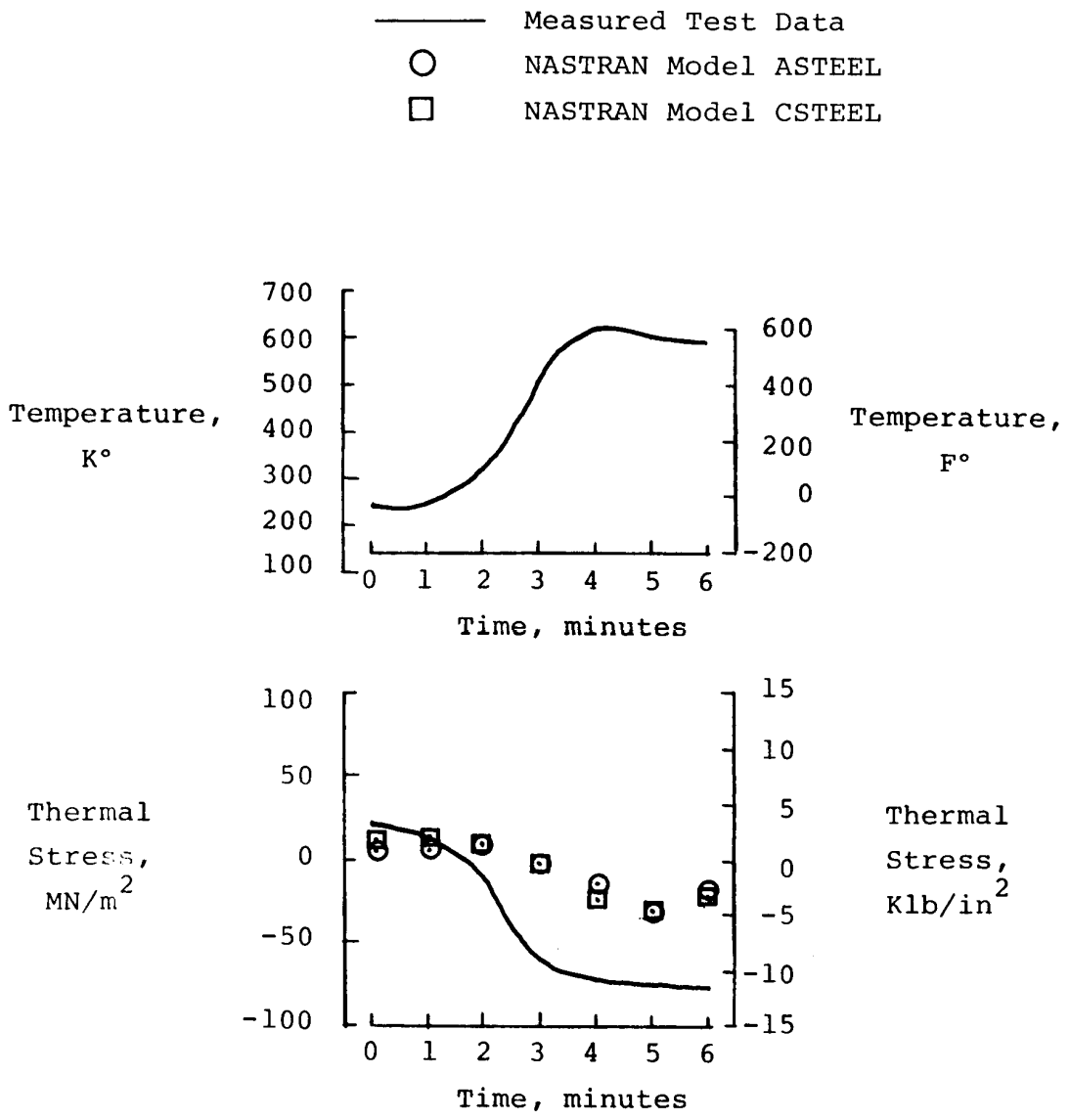

(b) Location CCC.

Figure 10. Continued.

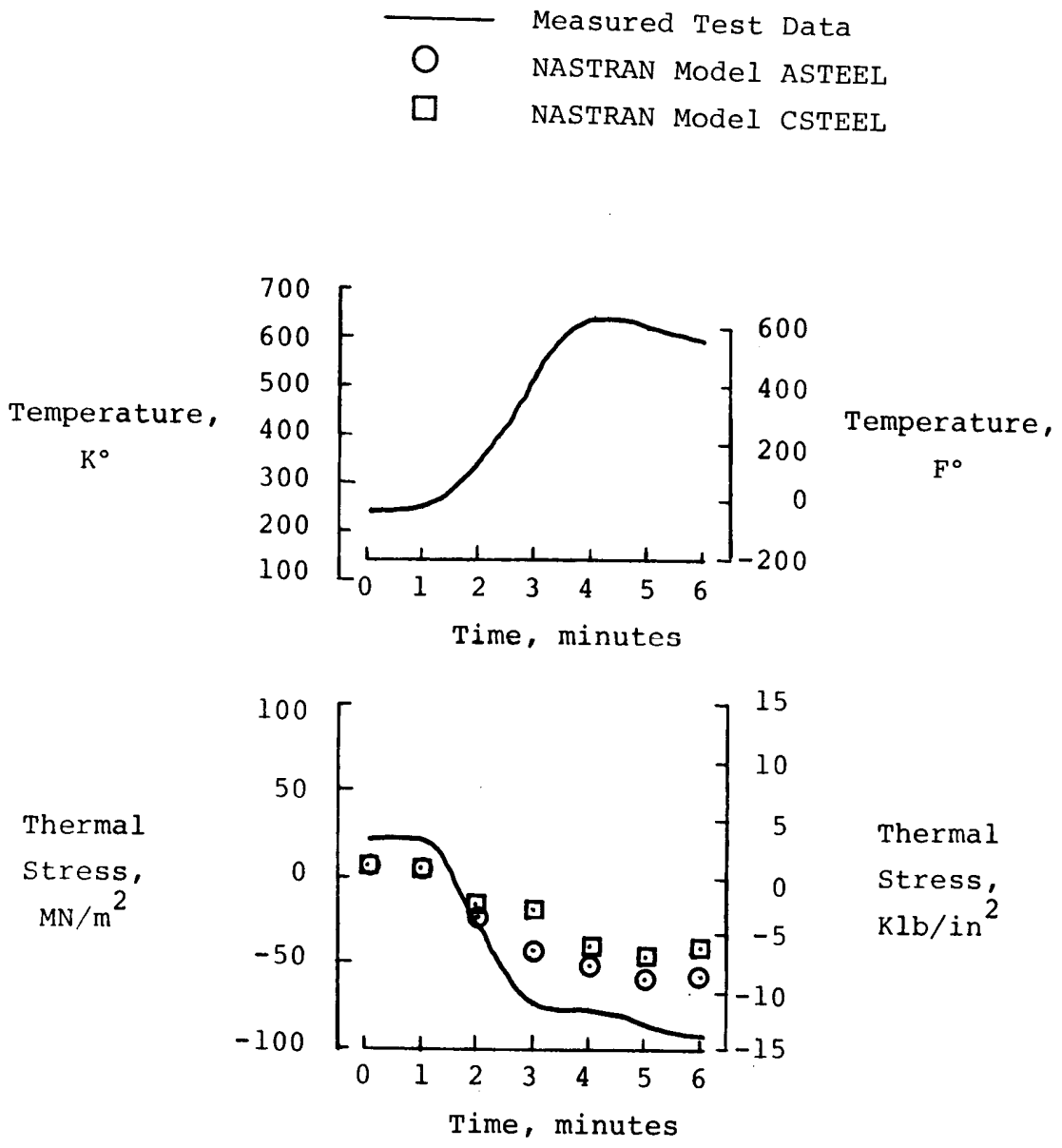

(c) Location EEE.

Figure 10. Continued.

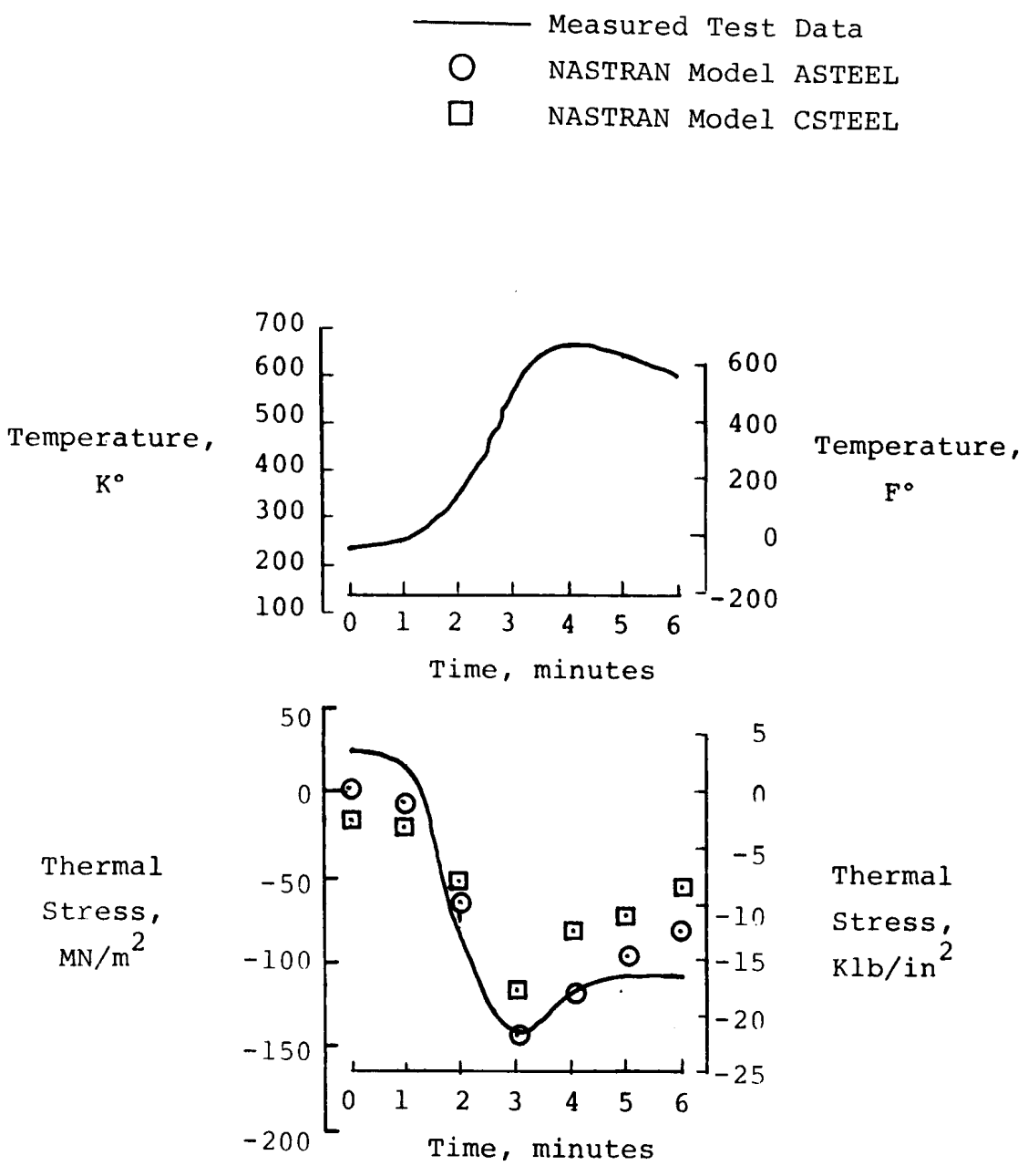

(d) Location GGG.

Figure 10. Continued.

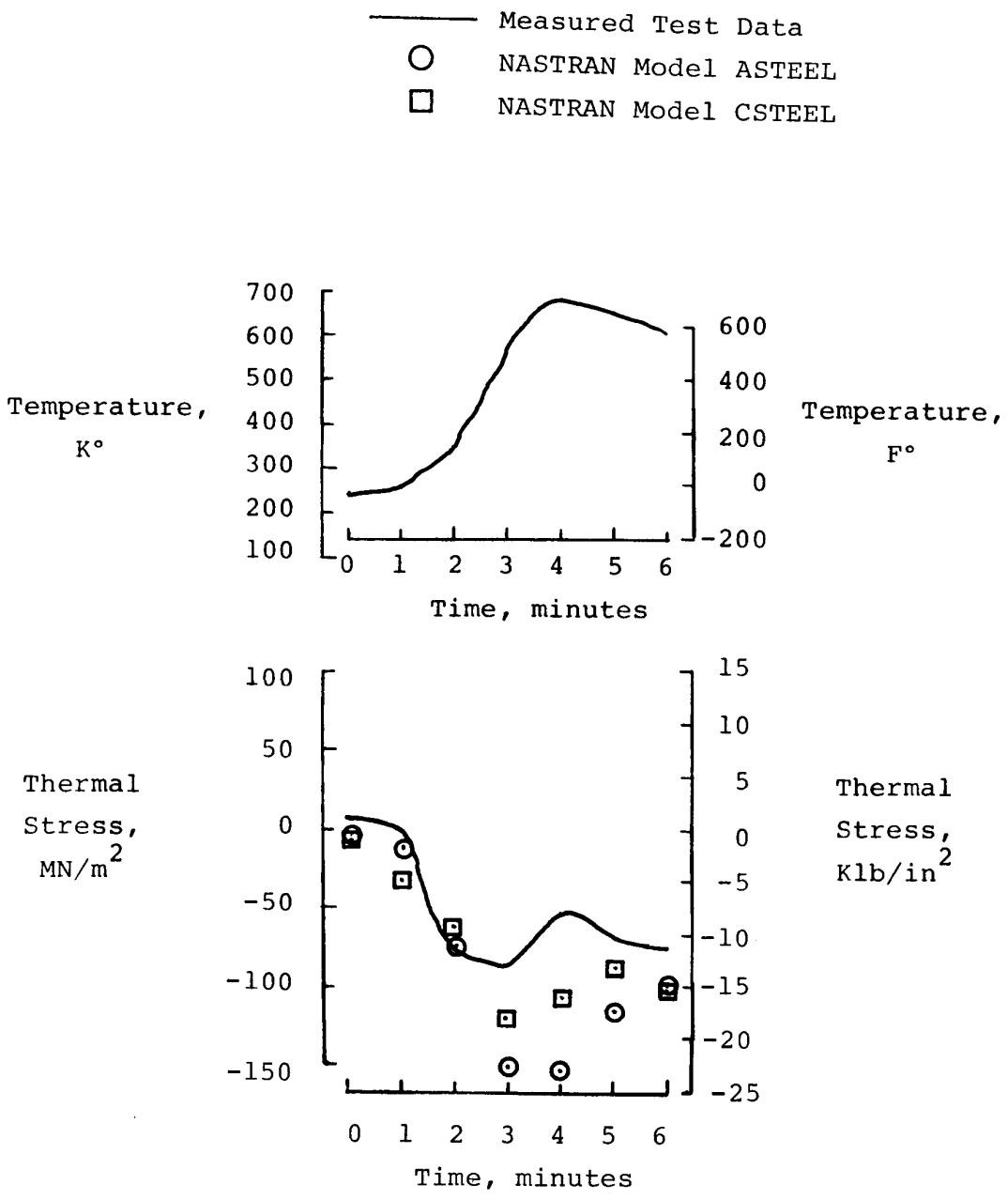

(e) Location III.

Figure 10. Continued.

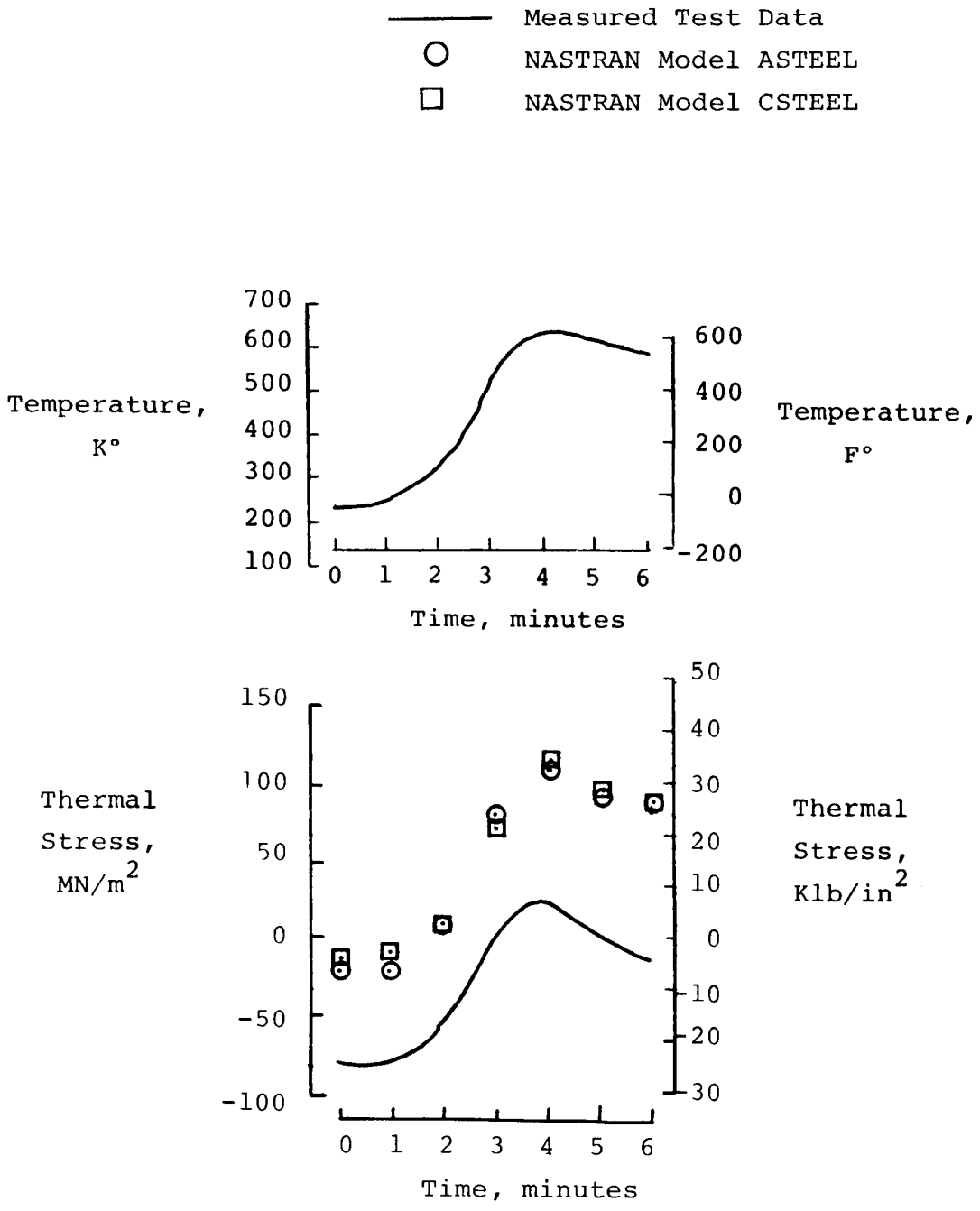

(f) Location MMM.

Figure 10. Continued.

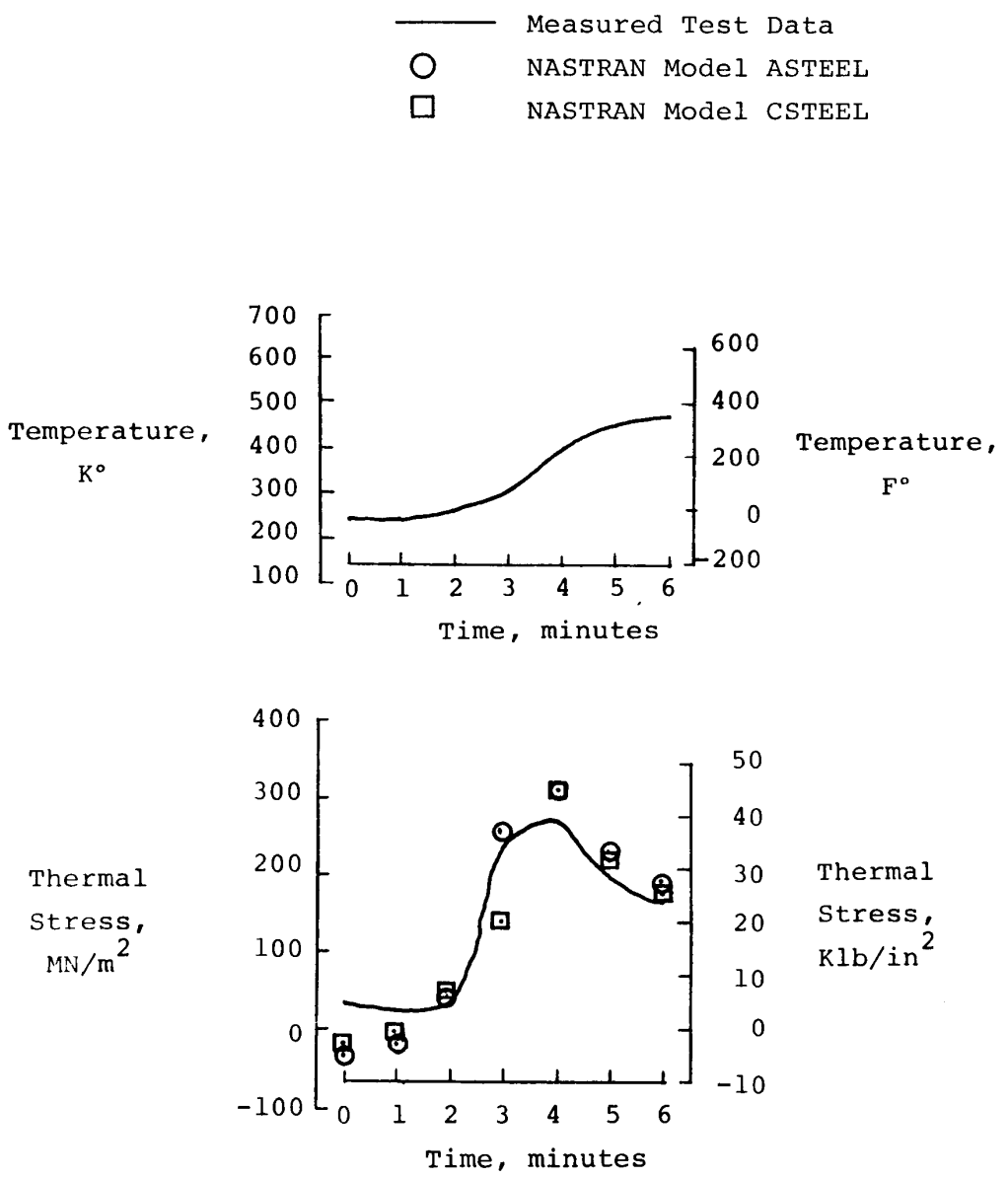

(g) Location NNN.

Figure 10. Continued.

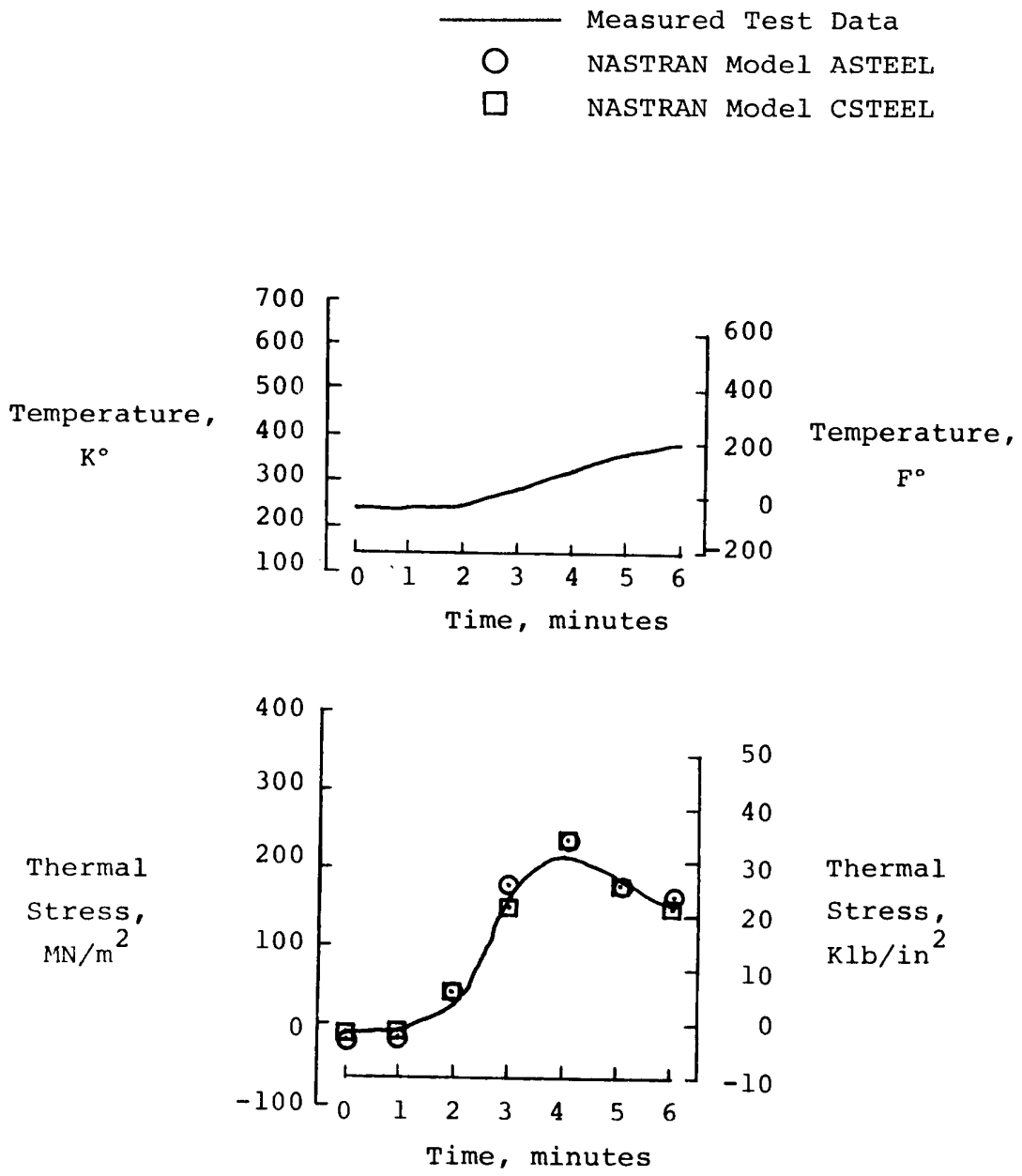

(h) Location OOO.

Figure 10. Continued.

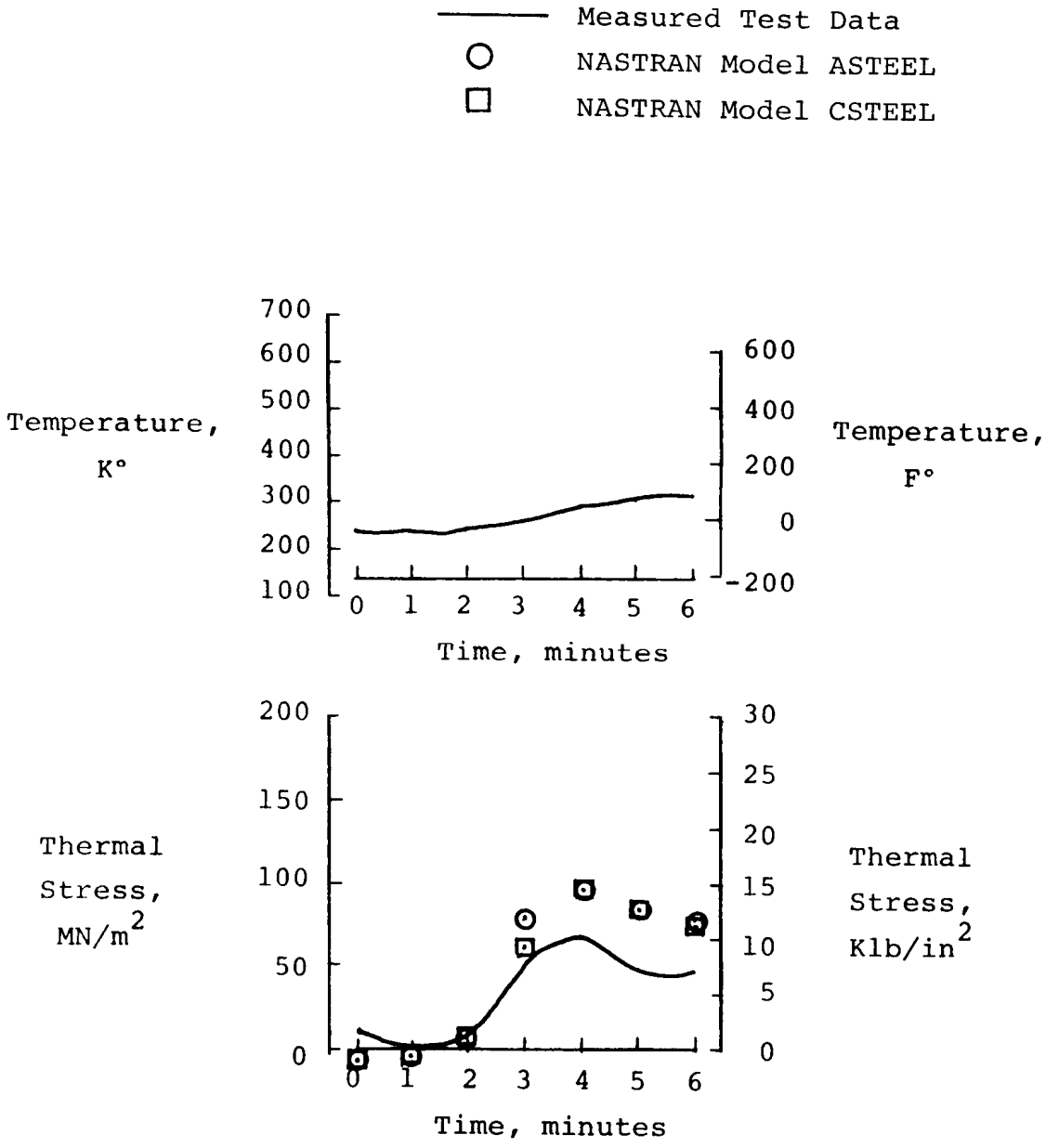

(i) Location PPP.

Figure 10. Continued.

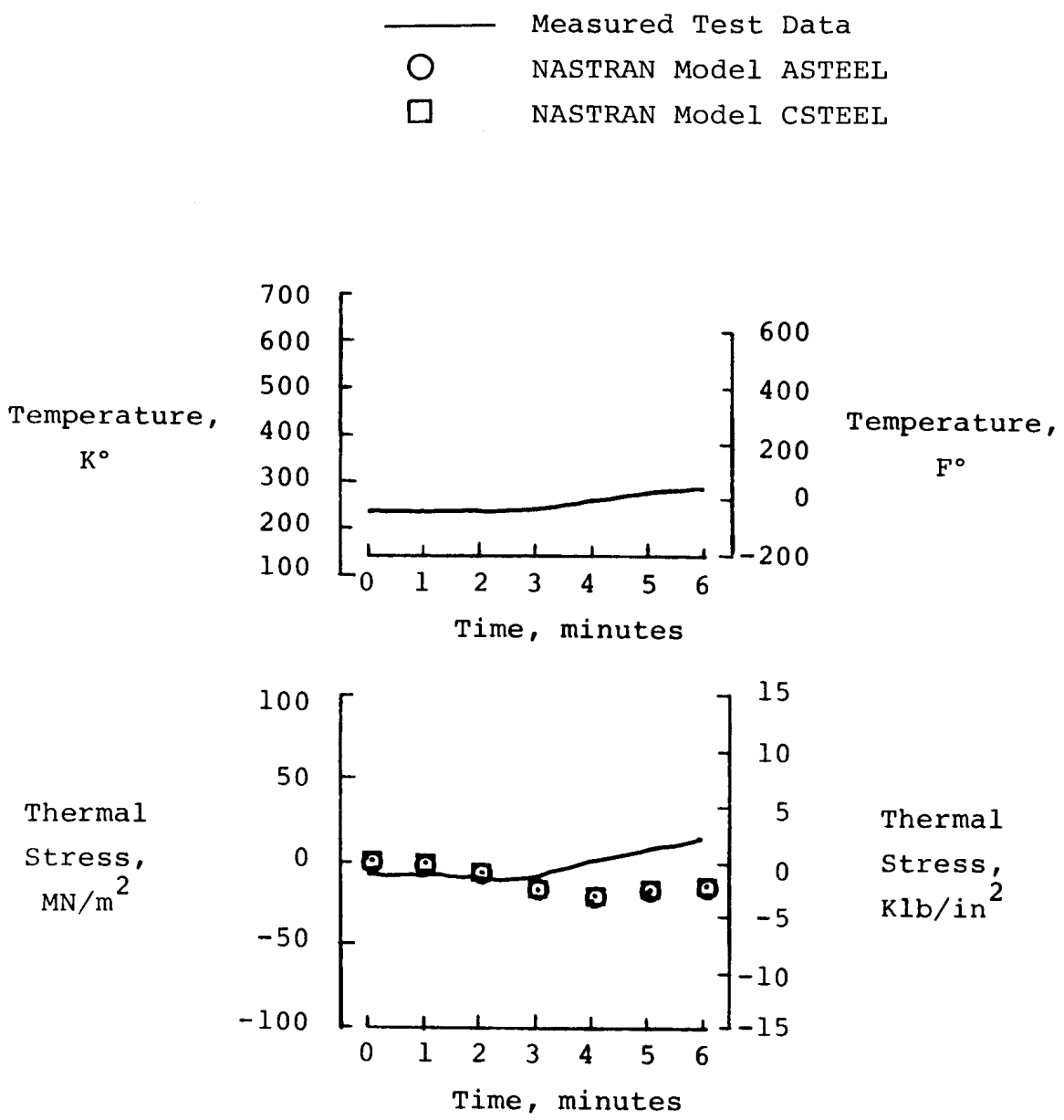

(j) Location QQQ.

Figure 10. Continued.

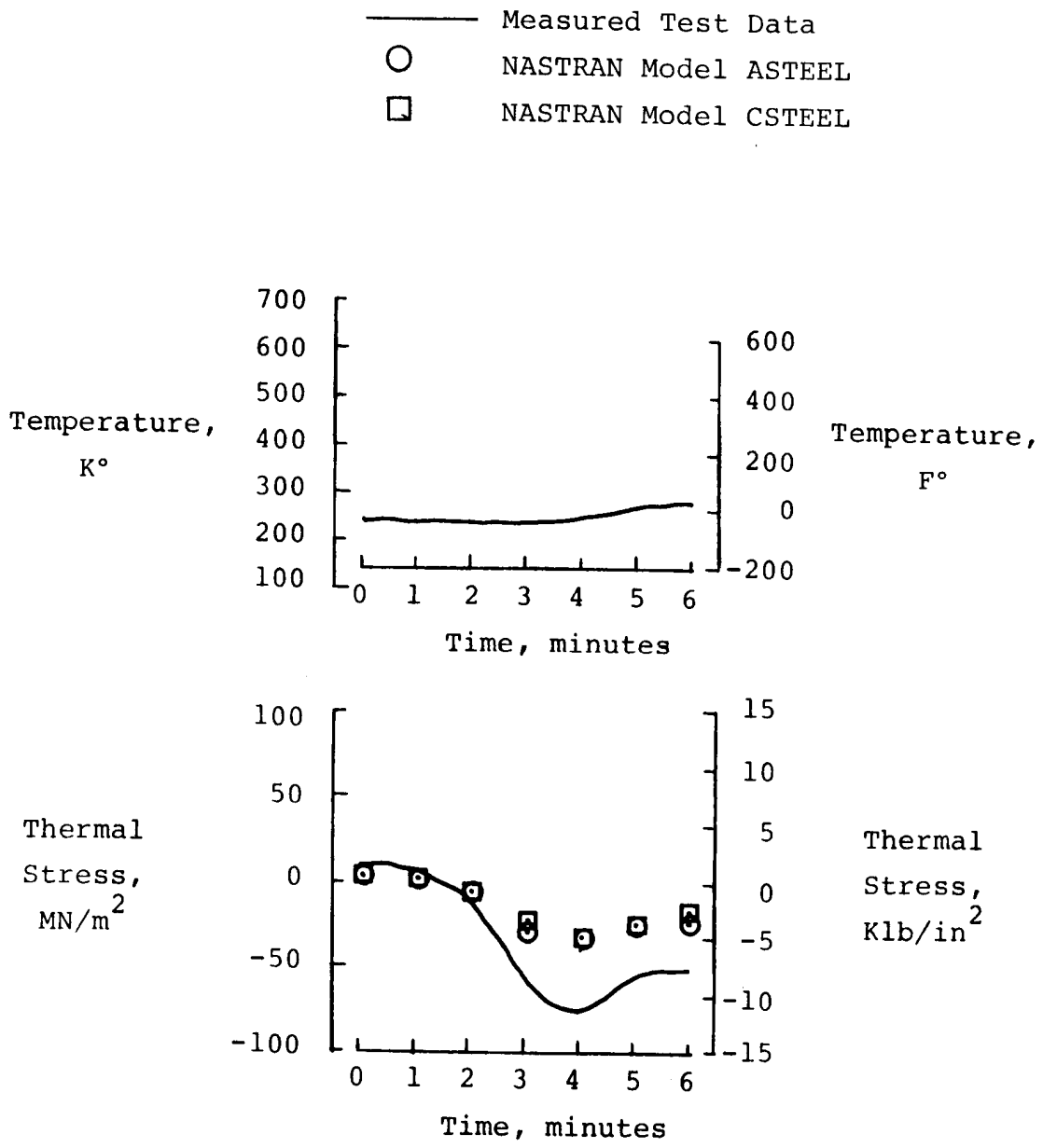

(k) Location RRR.

Figure 10. Continued.

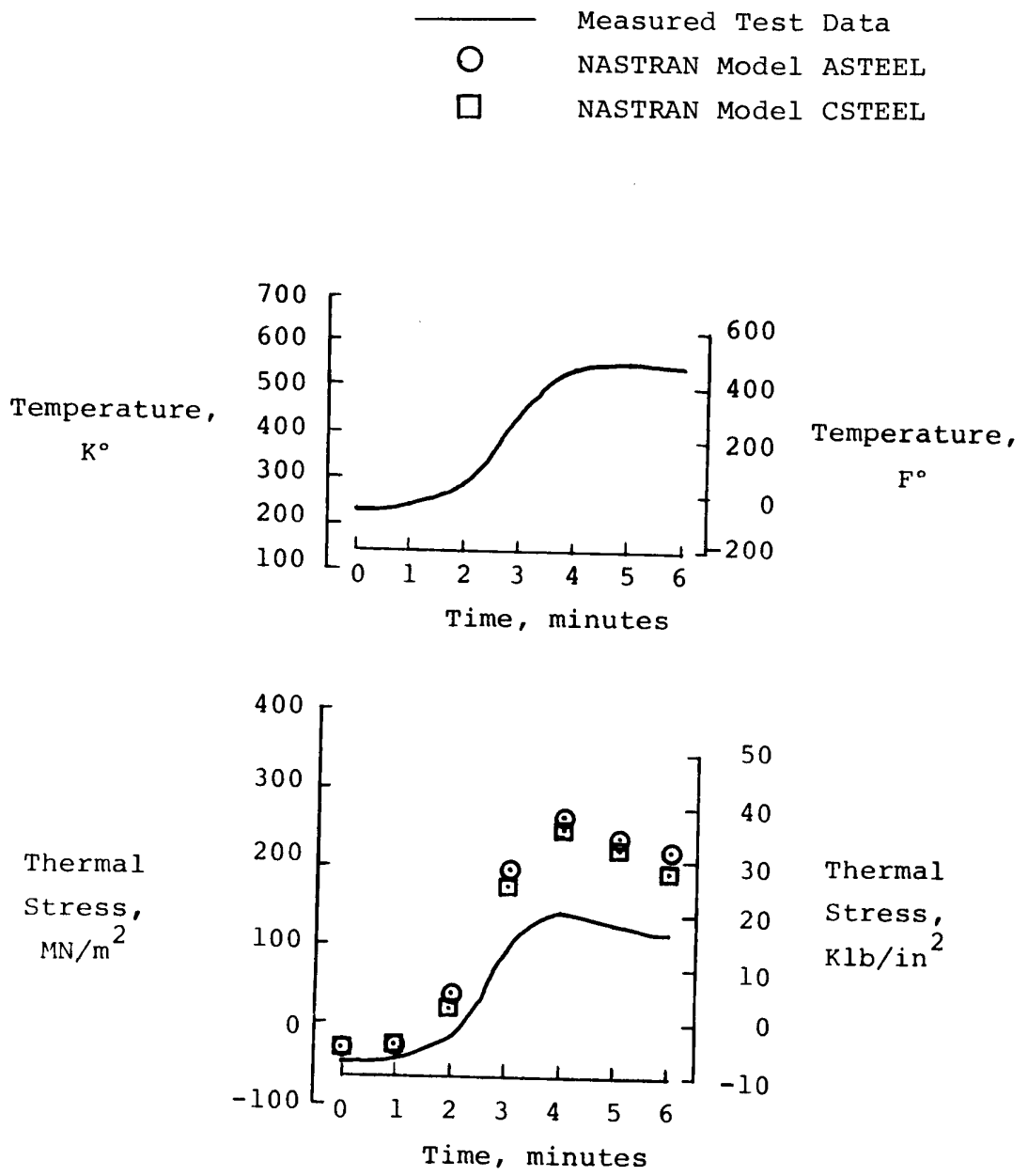

(l) Location SSS.

Figure 10. Continued.

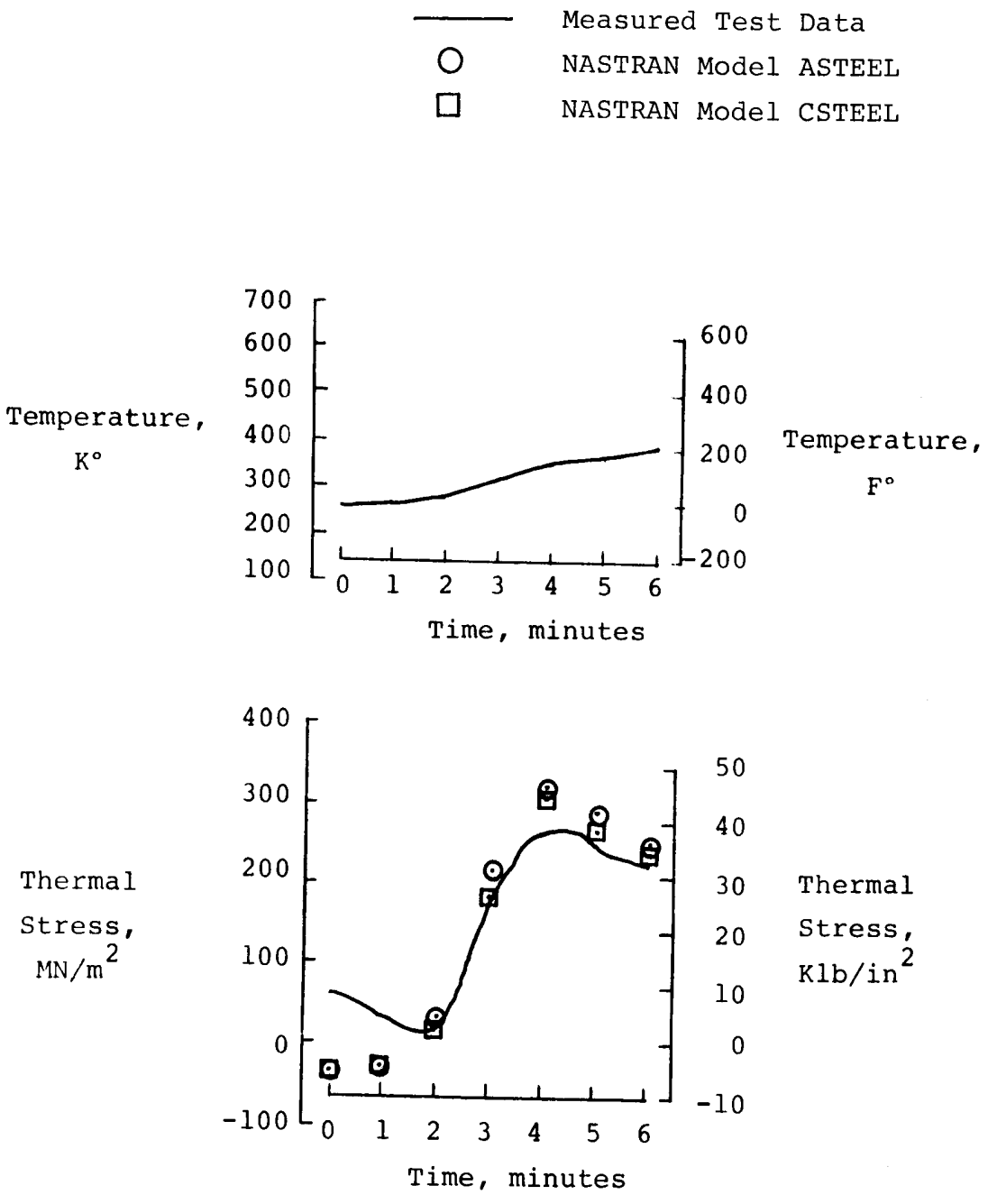

(m) Location TTT.

Figure 10. Continued.

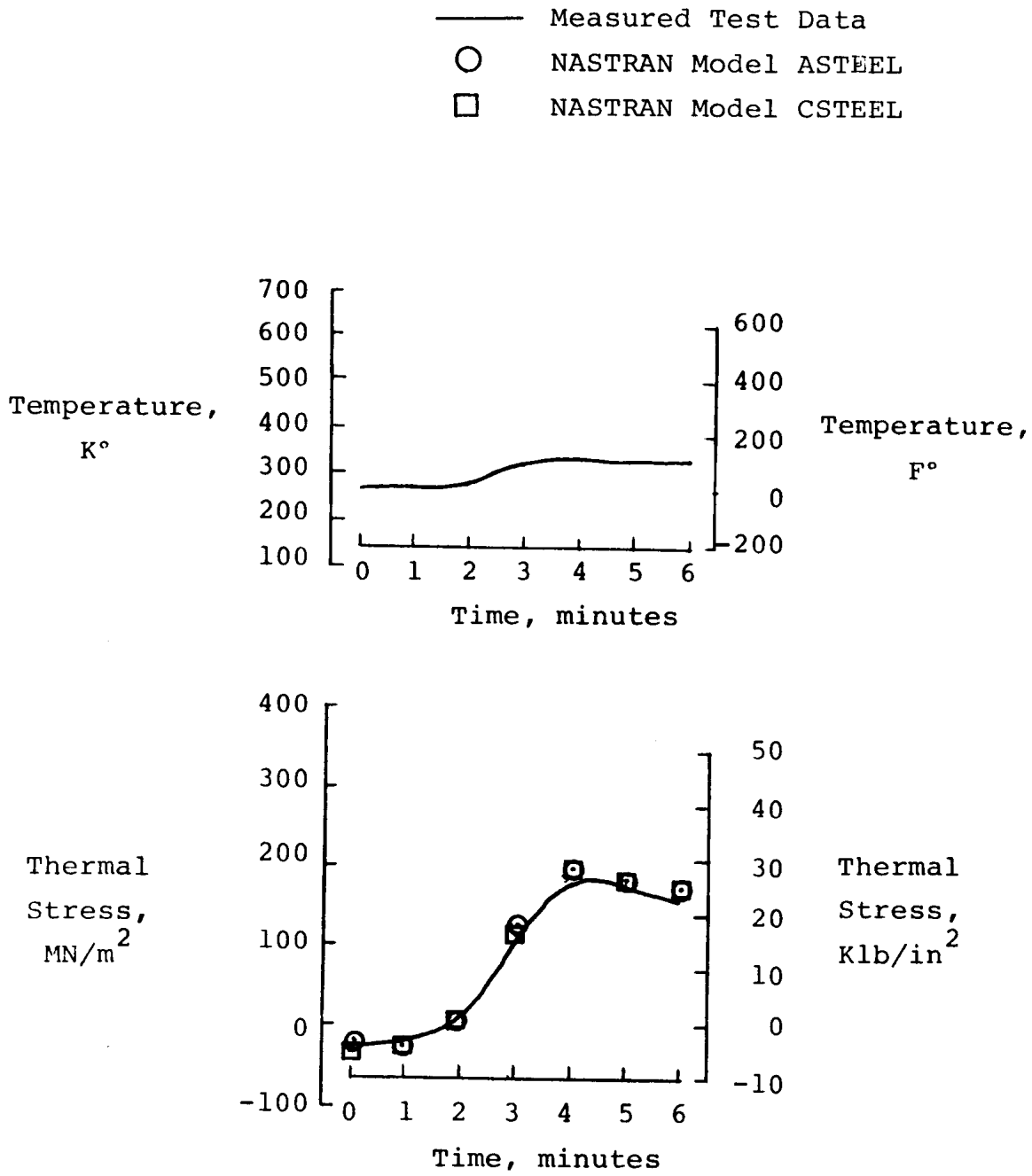

(n) Location UUU.

Figure 10. Continued.

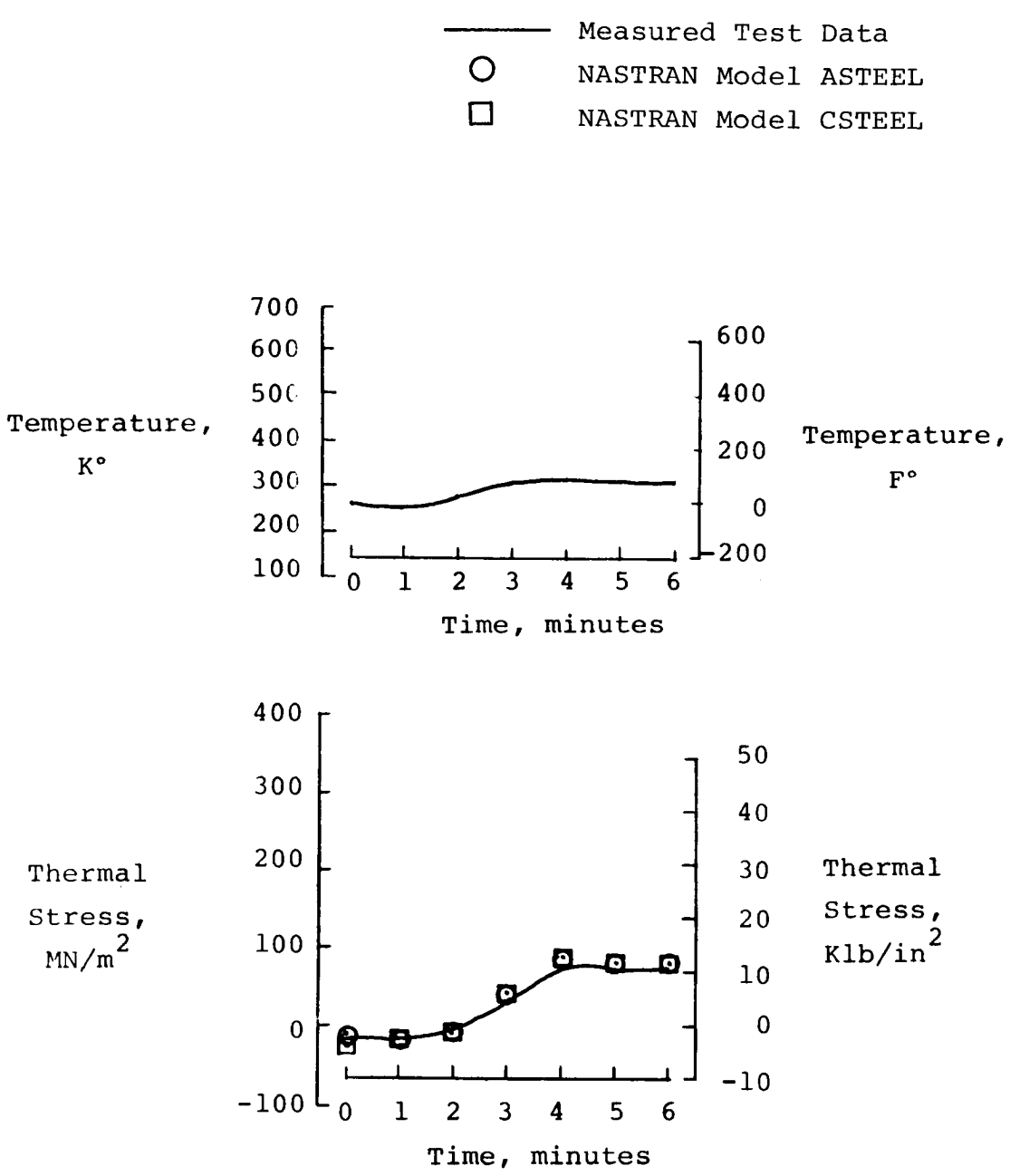

(o) Location VVV.

Figure 10. Continued.

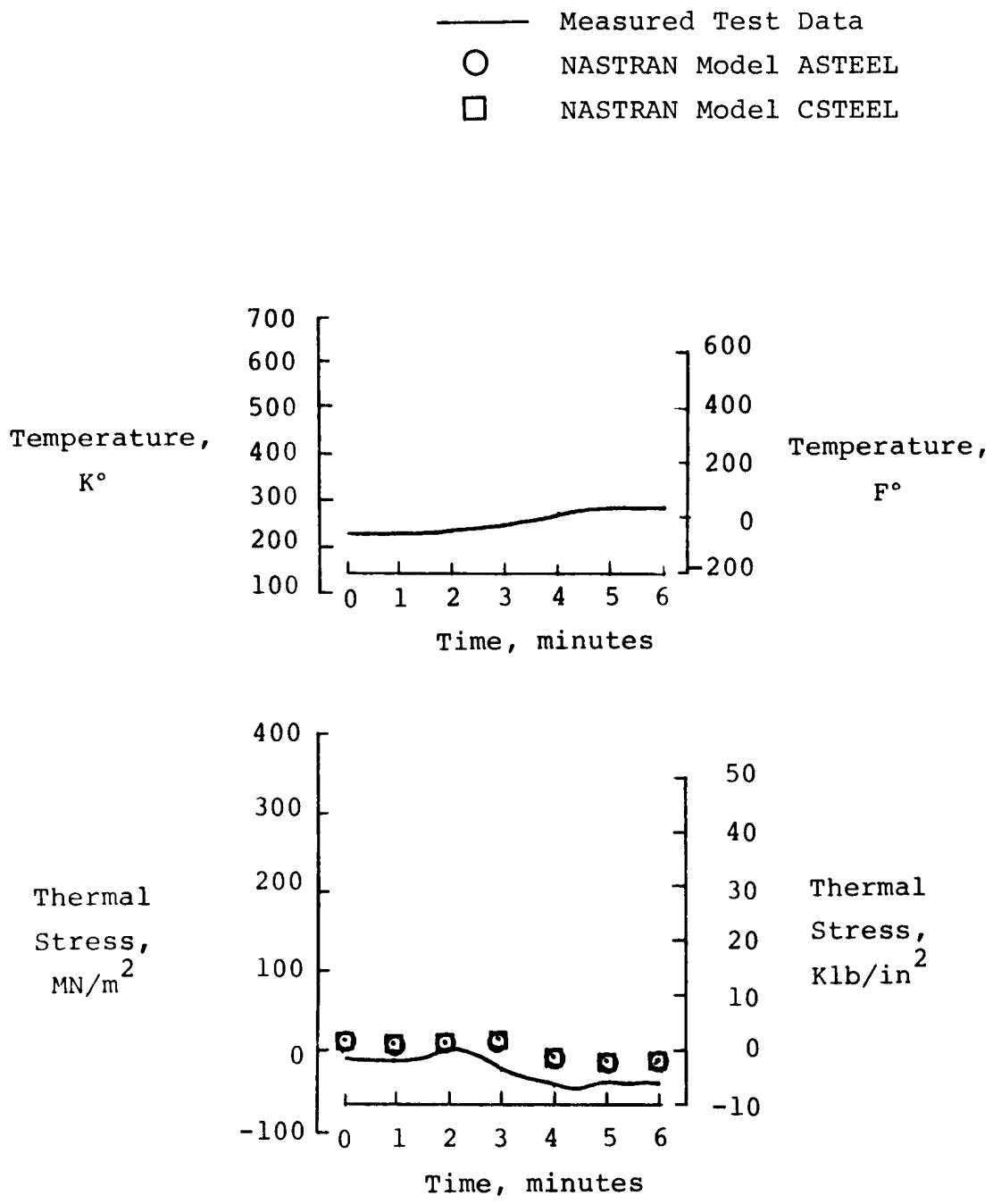

(p) Location WWW.

Figure 10. Continued.

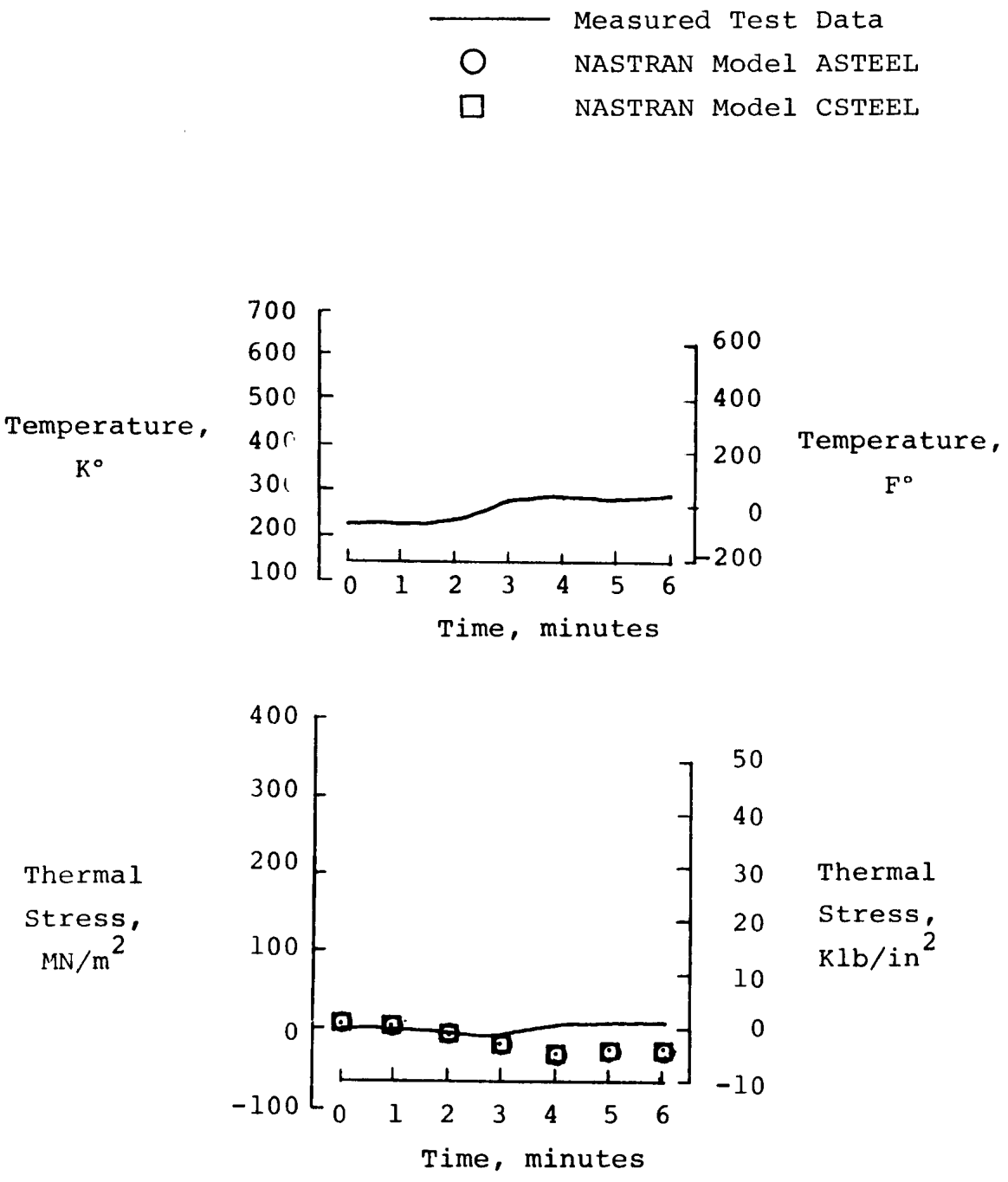

(q) Location XXX.

Figure 10. Concluded.

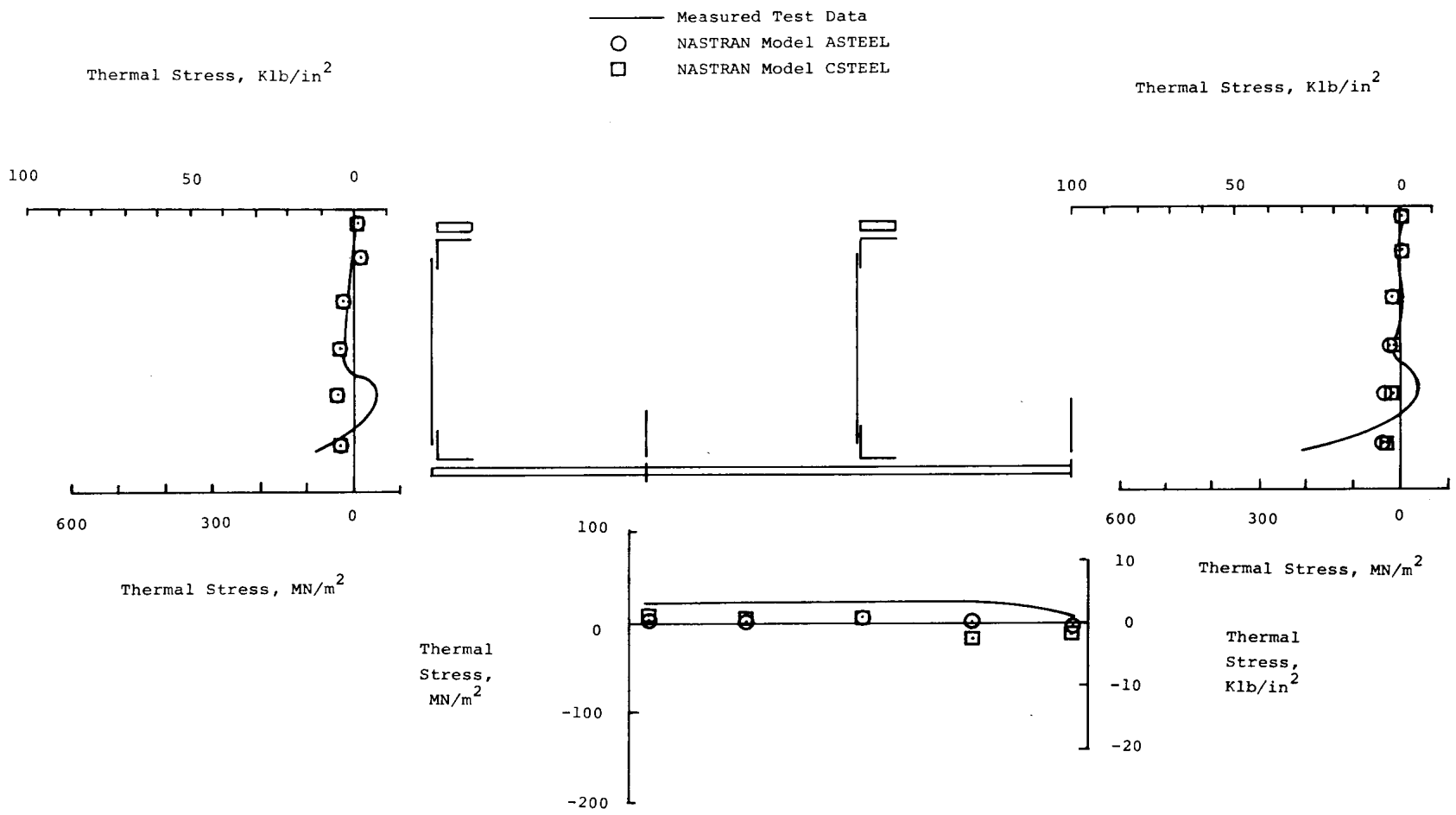

(a) Time = 0 minutes.

Figure 11. Comparison of measured and NASTRAN-calculated thermal stress distribution for the hypersonic profile.

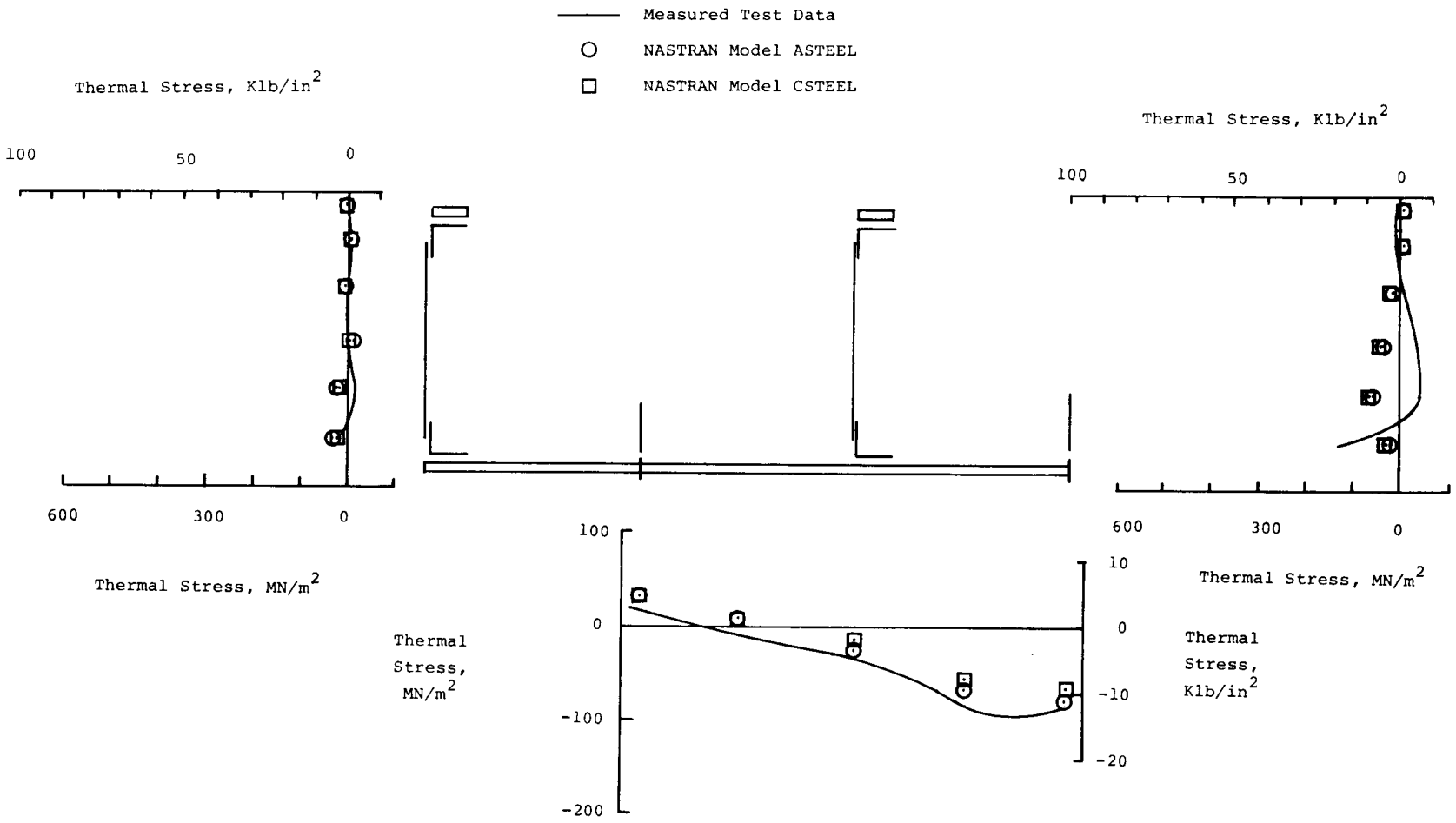

(b) Time = 2 minutes.

Figure 11. Continued.

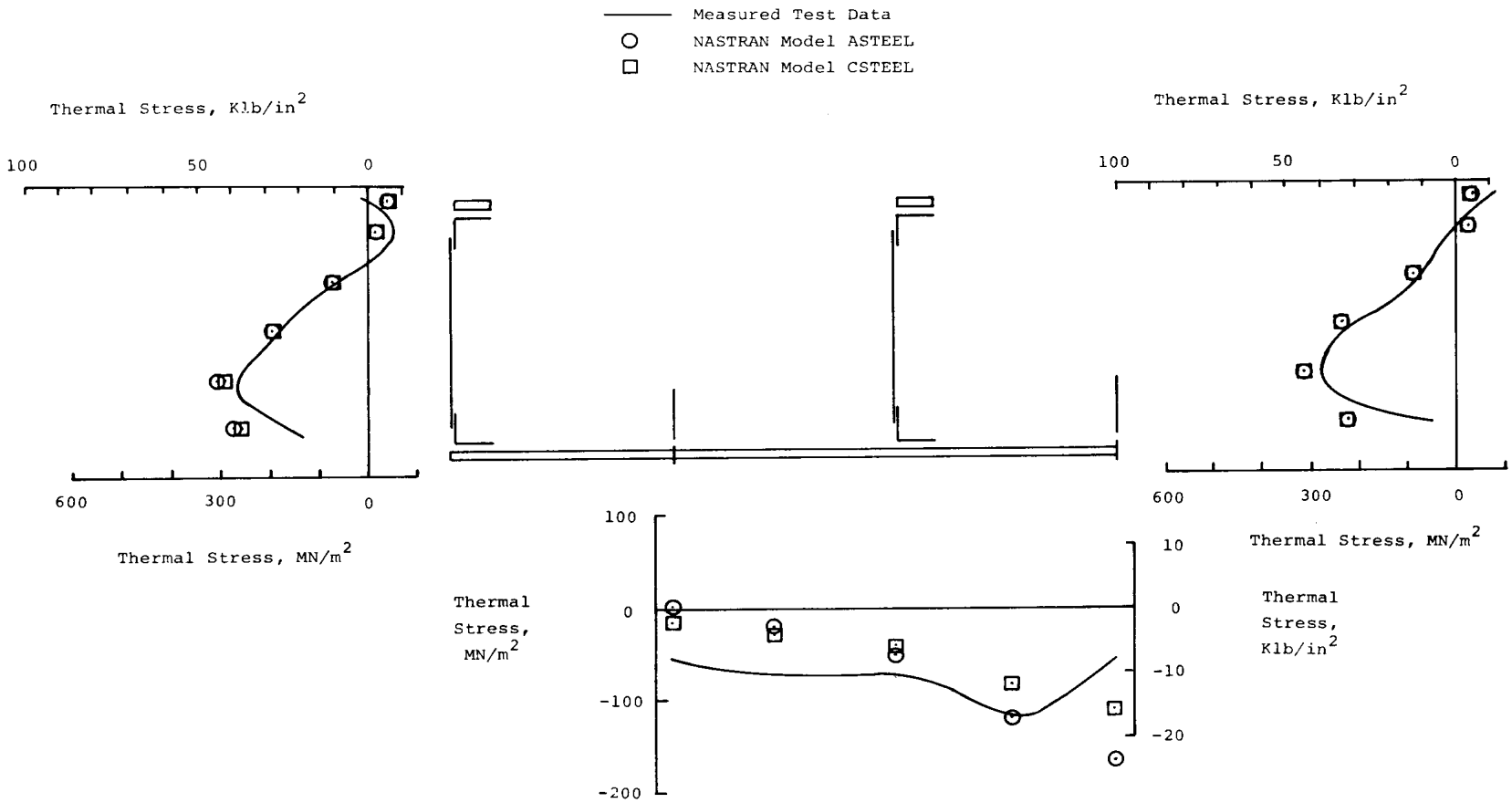

(c) Time = 4 minutes.

Figure 11. Continued.

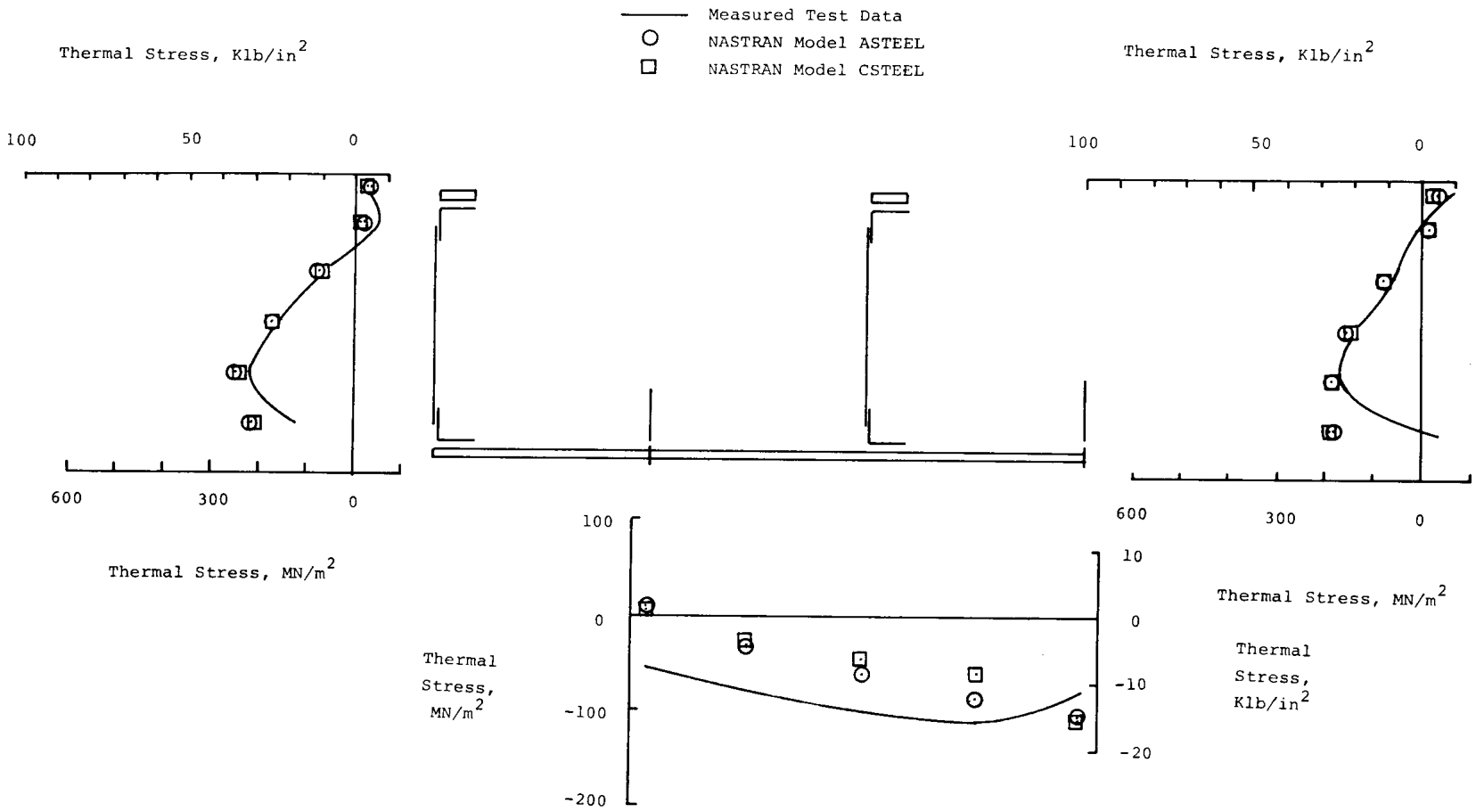

(d) Time = 6 minutes.

Figure 11. Concluded.

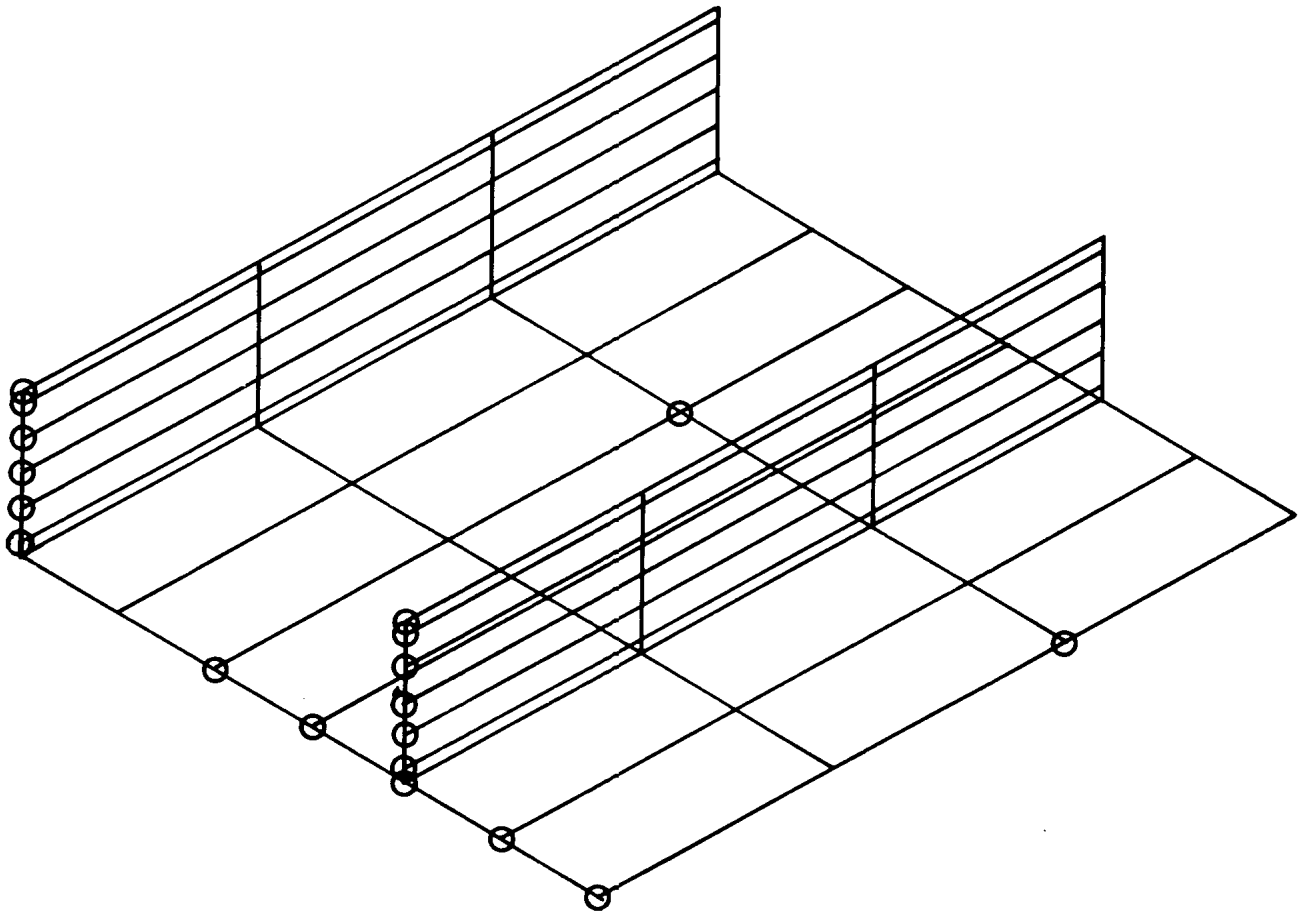

Figure 12. Location of thermocouples with respect to the NASTRAN structural model.

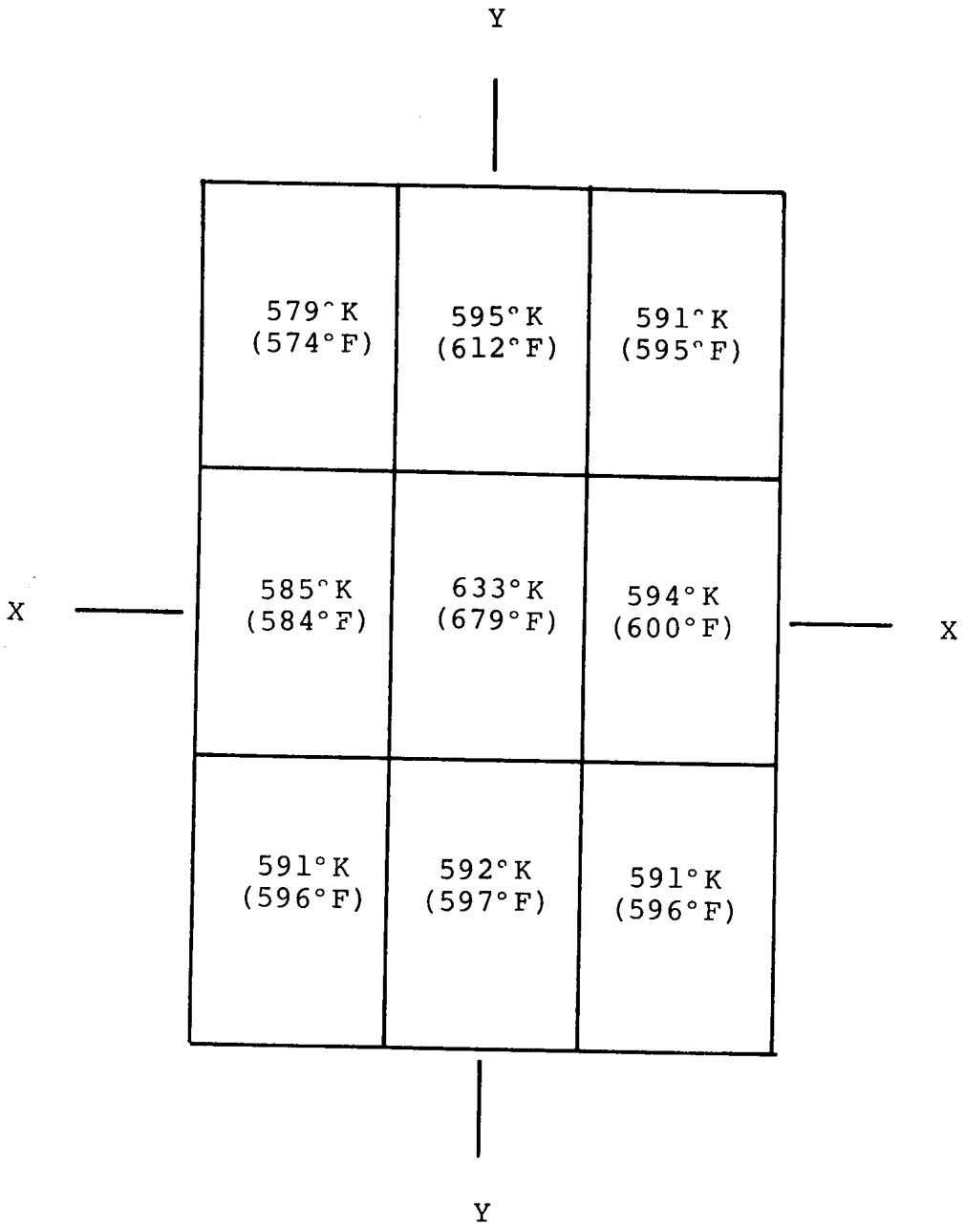

Figure 13. Temperature at each of the skin heating control zones for time = 4 minutes.

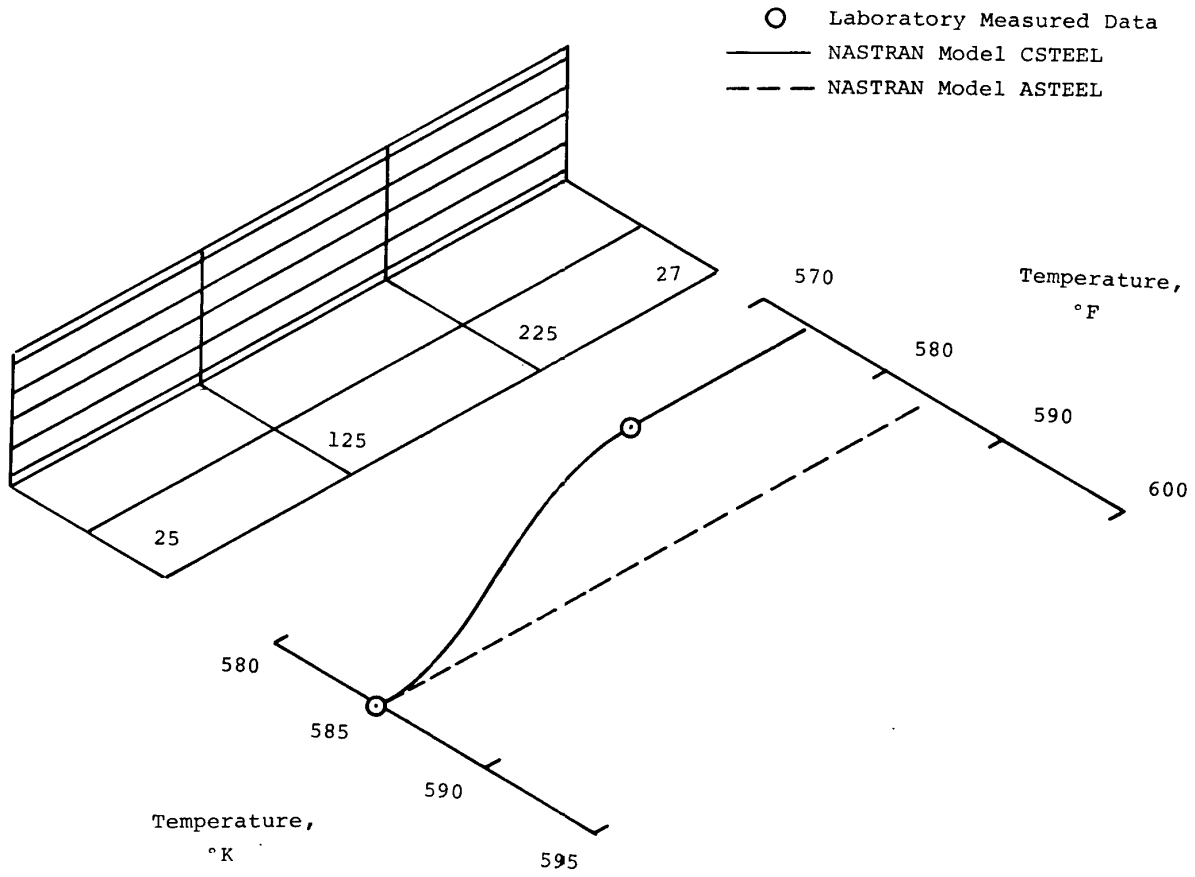

(a) Grid point 25 to grid point 27.

Figure 14. Illustration of longitudinal temperature smearing.

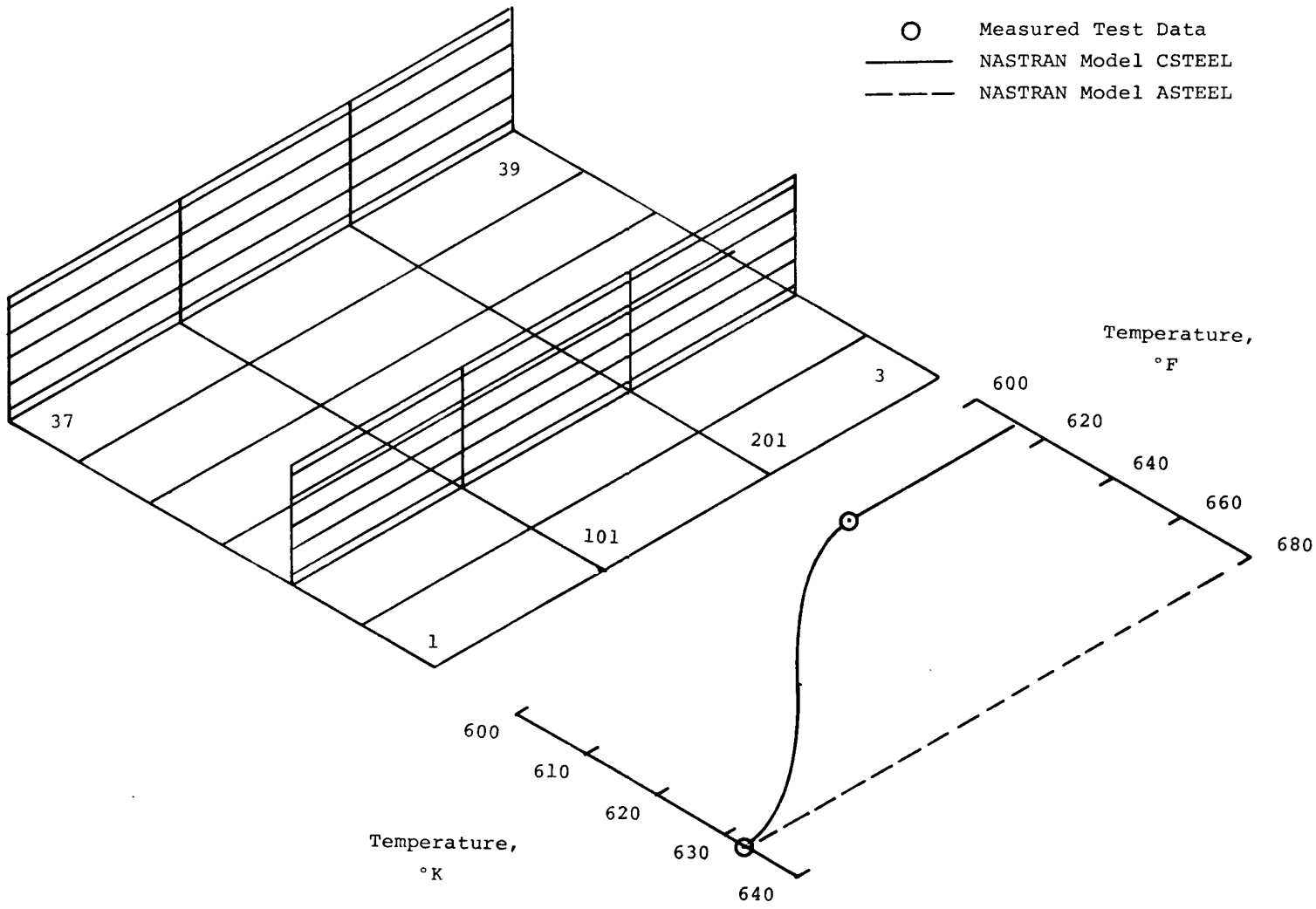

(b) Grid point 1 to grid point 3.

Figure 14. Concluded.

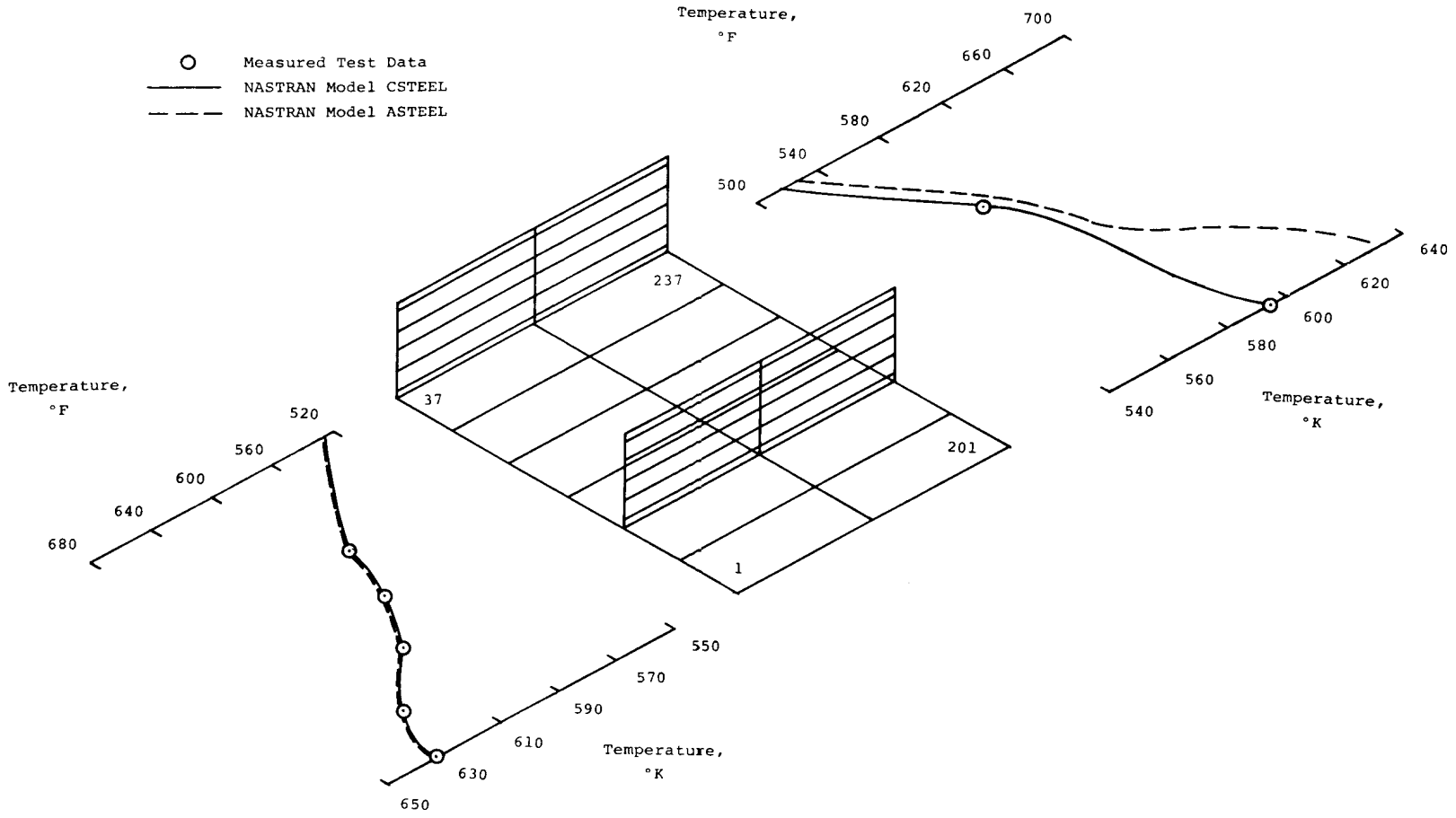

Figure 15. Illustration of the lateral temperature smearing.

1. Report No.	2. Government Accession No.	3. Recipient's Catalog No.
NASA TM-72865		

4. Title and Subtitle	5. Report Date
CORRELATION OF PREDICTED AND MEASURED THERMAL STRESSES ON AN ADVANCED AIRCRAFT STRUCTURE WITH DISSIMILAR MATERIALS	June 1979
	6. Performing Organization Code

7. Author(s)	8. Performing Organization Report No.
Jerald M. Jenkins	H-1092
	10. Work Unit No. 505-02-54

9. Performing Organization Name and Address	11. Contract or Grant No.
NASA Dryden Flight Research Center P.O. Box 273 Edwards, California 93523	
	13. Type of Report and Period Covered: Technical Memorandum

12. Sponsoring Agency Name and Address	14. Sponsoring Agency Code
National Aeronautics and Space Administration Washington, D.C. 20546	

15. Supplementary Notes

16. Abstract

A structure fabricated of dissimilar materials was investigated in terms of correlating measured and calculated thermal stresses. Additional information was added to a growing data base from which estimates of finite element model complexities can be made with respect to thermal stress analysis. The manner in which temperatures were smeared to the finite element grid points was examined from the point of view of the impact on thermal stress calculations.

The general comparison of calculated and measured thermal stresses is quite good and there is little doubt that the finite element approach provided by NASTRAN results in correct thermal stress calculations. Discrepancies did exist between measured and calculated values in the skin and the skin/frame junctures. The problems with predicting skin thermal stress were attributed to inadequate temperature inputs to the structural model rather than modeling insufficiencies. The discrepancies occurring at the skin/frame juncture were most likely due to insufficient modeling elements rather than temperature problems. In some areas, calculated thermal stresses varied considerably due to different temperature smearing approaches. It is apparent from the results of this paper, that thermal stresses calculated using the NASTRAN models are very sensitive to minor variations in the temperature input to the grid points.

17. Key Words (Suggested by Author(s))	18. Distribution Statement
Thermal stresses Hypersonic structures	Unclassified-Unlimited STAR category: 01

19. Security Classif. (of this report)	20. Security Classif. (of this page)	21. No. of Pages	22. Price*
Unclassified	Unclassified	48	$3.75

*For sale by the National Technical Information Service, Springfield, Virginia 22161